ORIGINAL RESEARCH

Inactivation of Interleukin-4 Receptor α Signaling in Myeloid Cells Protects Mice From Angiotensin II/High Salt–Induced Cardiovascular Dysfunction Through Suppression of Fibrotic Remodeling

Jianrui Song ![ID], PhD; Ryan A. Frieler, PhD; Thomas M. Vigil, BS; Jun Ma, MM; Frank Brombacher ![ID], PhD; Sascha N. Goonewardena, MD; Daniel R. Goldstein ![ID], MD*; Richard M. Mortensen ![ID], MD, PhD*

BACKGROUND: Hypertension-induced cardiovascular remodeling is characterized by chronic low-grade inflammation. Interleukin-4 receptor α (IL-4Rα) signaling is importantly involved in cardiovascular remodeling, however, the target cell type(s) is unclear. Here, we investigated the role of myeloid-specific IL-4Rα signaling in cardiovascular remodeling induced by angiotensin II and high salt.

METHODS AND RESULTS: Myeloid IL-4Rα deficiency suppressed both the in vitro and in vivo expression of alternatively activated macrophage markers including Arg1 (arginase 1), Ym1 (chitinase 3-like 3), and Relmα/Fizz1 (resistin-like molecule α). After angiotensin II and high salt treatment, myeloid-specific IL-4Rα deficiency did not change hypertrophic remodeling within the heart and aorta. However, myeloid IL-4Rα deficiency resulted in a substantial reduction in fibrosis through the suppression of profibrotic pathways and the enhancement of antifibrotic signaling. Decreased fibrosis was associated with significant preservation of myocardial function in MyIL4RαKO mice and was mediated by attenuated alternative macrophage activation.

CONCLUSIONS: Myeloid IL-4Rα signaling is substantially involved in fibrotic cardiovascular remodeling by controlling alternative macrophage activation and regulating fibrosis-related signaling. Inhibiting myeloid IL-4Rα signaling may be a potential strategy to prevent hypertensive cardiovascular diseases.

Key Words: fibrosis ■ hypertension ■ interleukin-4 receptor α ■ macrophage ■ remodeling

C ardiovascular remodeling occurs in response to pathological stimuli such as hypertension, which is characterized by molecular and cellular changes, including inflammation, hypertrophy, and fibrosis in targeted organs. The remodeling leads to structural changes within the heart and vasculature, resulting in cardiovascular dysfunction such as fatal cardiac arrhythmias.[1] Although the mechanisms underlying cardiovascular remodeling are yet to be fully elucidated, immune cells appear to play a critical role.[2,3] Immune cells coordinate the responses of multiple cell types during maladaptive remodeling and regulate cardiomyocyte function, scar formation, and fibrosis.[4] Modulating immune cell phenotypes, such as macrophage activation, has become an important target for modifying cardiovascular remodeling.

CLINICAL PERSPECTIVE

What Is New?

- Our study reveals that myeloid interleukin-4 receptor α (IL-4Rα) signaling is involved in profibrotic cardiovascular remodeling induced by angiotensin II and high salt, and myeloid-specific IL-4Rα deficiency preserves cardiac function by suppressing fibrosis.
- Myeloid IL-4Rα signaling controls alternative macrophage activation and fibrosis-related signaling.
- Myeloid cells are important cellular targets of endogenous IL-4Rα signaling.

What Are the Clinical Implications?

- Targeting myeloid IL-4Rα signaling may be a potential therapeutic strategy for hypertensive cardiovascular diseases.
- Developing therapies that are specific for IL-4Rα expressing cells in vivo could potentially develop novel therapies to treat hypertensive cardiovascular diseases.

Nonstandard Abbreviations and Acronyms

AAM	alternatively activated macrophage
AngII	angiotensin II
AngII/salt	angiotensin II and high salt
Arg1	arginase 1
CAM	classically activated macrophage
FC	floxed control
LPS	lipopolysaccharide
MMP	matrix metalloproteinase
MyIL4RαKO	myeloid-specific IL-4Rα knockout
Relmα/Fizz1	resistin-like molecule α
TGFβ	transforming growth factor β
TIMP1	tissue inhibitor of metalloproteinase 1
Ym1	chitinase 3-like 3

Macrophages are important contributors in acute and chronic cardiovascular remodeling.[5] There is a wide spectrum of macrophage activation with 2 extremes: classically activated macrophages (CAMs/M1-like) and alternatively activated macrophages (AAMs/M2-like). AAMs are often anti-inflammatory and reparative; however, AAMs can also be detrimental. For instance, AAMs are profibrotic and have been associated with increased injury in hypoxia-induced pulmonary hypertension.[6] Interleukin (IL)-4 and IL-13 are cytokine inducers of AAMs that share

the same receptor subunit IL-4 receptor α (IL-4Rα). IL-4Rα signaling promotes fibrosis as IL-4Rα^{-/-} mice and IL-4/IL-13 double knockout mice exhibit decreased fibrosis in pancreatitis.[7] IL-4-deficient mice show reduced cardiac fibrosis and improved cardiac function during angiotensin II (AngII)–induced cardiac injury and inflammatory dilated cardiomyopathy.[8,9] Similarly, neutralizing IL-4 significantly decreases hypertrophy and fibrosis.[10] However, as IL-4Rα is widely expressed on a variety of cell types such as T cells,[11] B cells, monocytes/macrophages, neutrophils,[12–14] fibroblasts,[15] endothelial cells, smooth muscle cells,[16] and cardiomyocytes,[17] the critical cell type by which IL-4 conveys the profibrotic response has not yet been identified.

Here we used myeloid-specific IL-4Rα knockout (MyIL4RαKO) mice to delineate the role of IL-4Rα signaling in myeloid cells during AngII and high salt (AngII/salt)–induced cardiovascular remodeling. We hypothesize that (1) myeloid IL-4Rα signaling promotes fibrosis in cardiovascular remodeling by enhancing AAM polarization and (2) that abolishing IL-4Rα in myeloid cells reduces cardiovascular fibrosis and results in cardiovascular protection.

METHODS

The authors declare that all supporting data are available within the article and its online supplementary files.

Animals

Male MyIL4RαKO (IL-4Rα[flox/flox]-LysMCre) and littermate floxed control (FC; IL-4Rα[flox/flox]) mice on a C57BL/6 background were used for the AngII/salt-induced hypertensive injury model.[18] We only used male mice, which is a limitation of the study. Male 10- to 12-week-old mice were randomly assigned to treatment (AngII and 4% NaCl diet) and sham groups. Depending on specific experiments, between 5 to 20 FC or MyIL4RαKO mice were included in each group. Mice in the treatment group were infused with AngII (1.5 mg/kg per day, Sigma-Aldrich, Catalog No. A9525) using an osmotic pump (Alzet, Model 1002) and administered a 4% NaCl diet (Envigo, Catalog No. TD.03095) for 4 weeks while sham mice were implanted with osmotic pumps containing vehicle control (saline) and were administered a standard diet (LabDiet, 5L0D). Noninvasive blood pressure measurements were performed using an IITC Life Science tail cuff plethysmography blood pressure system at the end of the experiments. All animal procedures were performed in accordance with the *Guide for the Care and Use of Laboratory Animals* (8th edition) and were approved by the Institutional Animal Care and Use Committee of the University of Michigan.

Peritoneal Macrophages

Peritoneal macrophages were isolated 4 days after intraperitoneal injection of thioglycolate and then cultured in DMEM (Gibco, Catalog No. 11965-092) containing 10% fetal bovine serum and 100 units/mL penicillin and 100 mg/mL streptomycin in a humidified incubator under 95% air and 5% CO_2 at 37°C. Alternative macrophage activation was induced with IL-4 (50 ng/mL) for 24 hours, and classical macrophage activation was induced with lipopolysaccharide (LPS; 100 ng/mL) for 3 hours.

Histological Analysis

Hearts and aortas were fixed in 4% paraformaldehyde for 48 hours and then paraffin processed and embedded for histological analysis. Transverse tissue sections (5 μm) were subjected to hematoxylin-eosin staining and imaged using a Zeiss Axio Imager 2 microscope (Carl Zeiss). For determination of the myocyte cross-sectional area, myocytes with similar-sized nuclei and intact cellular membranes were outlined by a blinded observer, and the myocyte cross-sectional area was calculated using ImageJ 1.45s software. The average myocyte cross-sectional area was calculated from multiple images and from around 200 myocytes per heart. To determine wall thickness and the medial area of aorta, perpendicular lines were drawn from internal elastic lamina to the external lamina at a minimum of 10 locations per aorta section to measure the distance, and the average distance was calculated as the wall thickness of the aorta.[19] For the medial area, the internal and external perimeters of the elastic laminas were traced, and the area between those 2 perimeters was quantified and reported as the aortic medial wall area. To determine fibrosis, tissue sections of the heart, aorta, and kidney were stained by picrosirius red as described previously.[19,20] ImageJ was used to quantify fibrosis. Immunohistochemical staining for Arg1 (arginase1; Invitrogen, Catalog No. PA5-29645) and Ym1 (chitinase 3-like 3; R&D Systems, Catalog No. AF2446) were performed on heart sections. Pictures were taken of all regions in the stained sections. Positively stained areas and the total area were traced and measured with ImageJ, and the percentage of Arg1-positive or Ym1-positive areas was calculated.

Gene Expression Analysis

Relative mRNA expression was determined using quantitative reverse transcription–polymerase chain reaction. Total RNA was extracted with TRIzol reagent and RNA was reverse transcribed to cDNA with a High-Capacity cDNA Reverse Transcription Kit (Applied Biosystems). Quantitative polymerase chain reaction was performed using a 7900HT fast real-time polymerase chain reaction system (Applied Biosystems), and relative mRNA expression was analyzed using the comparative method and normalized to the internal control *L32*.

Echocardiography

Mice were anesthetized with isoflurane, and echocardiography was performed using a Vevo 2100 Micro-Imaging System (VisualSonics Inc.) with an 18-MHz to 38-MHz linear array ultrasound transducer. The acquisition and analysis were done by a single experienced researcher in a blinded manner. Systolic and diastolic dimensions were determined by M-mode in the parasternal short axis view at the level of the papillary muscles. Ejection fraction, fractional shortening, left ventricle (LV) end systolic and diastolic diameters, LV end systolic and diastolic volumes, and systole and diastole LV posterior wall thicknesses were calculated based on the M-mode parasternal short axis view. Systolic and diastolic LV area and ascending aorta diameter were determined by the 2-dimensional long axis view. Aorta velocity peak gradient was measured by conventional pulsed-wave spectral Doppler analysis of mitral valve inflow patterns.

Flow Cytometric Analysis and Sorting

Single-cell suspensions from the heart and aorta were prepared by mincing tissues followed by enzymatic digestion with collagenase I (450 U/mL), collagenase XI (125 U/mL), DNase I (60 U/mL), and hyaluronidase (60 U/mL) for 1 hour at 37°C with agitation.[21] Single-cell suspensions from the blood and spleen were prepared after red blood cell lysis. Total viable cell counts were performed using Trypan Blue. Cells were then blocked by incubating with anti–cluster of differentiation (CD) 16/32 (Biolegend, Catalog No. 101302) for 5 minutes on ice. Cells were then incubated with antibodies on ice (light protected) for 30 minutes. The anti-TNFα-PE/Dazzle 594 was incubated for 30 minutes on ice after cell permeabilization (eBioscience, Catalog No. 88-8824) and fixation. Following are the antibodies used: anti-CD45-PerCP/Cyanine 5.5 (Biolegend, Catalog No. 103131), anti-CD45-PE/Cyanine7 (Biolegend, Catalog No. 103113), anti-CD45-Pacific Blue (Biolegend, Catalog No. 103126), anti-CD11b-Brilliant Violet 605 (Biolegend, Catalog No. 101257), anti-F4/80-PE (Biolegend, Catalog No. 123110), anti-CD206-Alexa Fluor 488 (Biolegend, Catalog No. 141710), anti-TNFα-PE/Dazzle 594 (Biolegend, Catalog No. 506345), anti-CD3-APC (Biolegend, Catalog No. 100235), anti-Ly6G-FITC (Biolegend, Catalog No. 127605), anti-Ly6C-PerCP/Cyanine5.5

(Biolegend, Catalog No. 128011), and anti-IL-4Rα-APC (Biolegend, Catalog No. 144807). Flow cytometry was performed using a BD LSRFortessa flow cytometer (BD Biosciences), and data were analyzed using FlowJo V10.1 software. Macrophages were identified as CD45+CD11b+F4/80+, neutrophils were identified as CD45+CD11b+Ly6G+, T cells were identified as CD45+CD3+, monocytes were identified as CD45+CD11b+Ly6C+Ly6G−, and monocytes were further divided into Ly6C^{low} and Ly6C^{high} populations based on the expression of Ly6C. Total cell numbers were normalized to tissue weight for analysis. Cell sorting was performed using MoFlo Astrios Cell Sorter.

Western Blotting

Protein was extracted from indicated tissues in lysis buffer (Thermo Fisher Scientific, Catalog No. 78510) with a protease inhibitor cocktail (Sigma, Catalog No. P8340) and a phosphatase inhibitor cocktail (Sigma, Catalog No. P5726) using a tissue homogenizer (PRO Scientific). Equal amounts of protein were separated by SDS-PAGE and transferred to a polyvinylidene fluoride membrane. After blocking with 5% BSA buffer, the membrane was probed with anti-MMP (matrix metalloproteinase) 3 (Abcam, Catalog No. ab52915), anti-MMP10 (Abcam, Catalog No. ab199688), and anti-TIMP1 (tissue inhibitor of metalloproteinase 1; Abcam, Catalog No. ab179580) and then developed with chemiluminescent substrate (Thermo Fisher Scientific, Catalog No. 34577). Anti-GAPDH (Cell Signaling, Catalog No. 2118) was used as internal control to guarantee equal protein loading.

Statistical Analysis

Results are presented as mean±SEM. Normality was determined using the Shapiro-Wilk test. Student *t* test and 2-way ANOVA followed by Tukey's post hoc test were used for data that are normally distributed, and nonparametric tests including the Mann-Whitney and Kruskal-Wallis tests were used for data that are not normally distrubuted. All statistical analyses of data were performed in GraphPad Prism (version 8; GraphPad Software, Inc). *P*<0.05 was considered significant.

RESULTS

Myeloid-Specific IL-4Rα Deficiency Suppresses Alternatively Activated Macrophage Polarization In Vitro

To investigate the role of myeloid IL-4Rα signaling during AngII/salt-induced cardiovascular remodeling, we established a myeloid-specific IL-4Rα knockout murine model using LysM promoter-driven cre recombination. First, we verified the knockout efficiency by measuring IL-4Rα at the mRNA level by quantitative reverse transcription–polymerase chain reaction and at the protein level by flow cytometry in peritoneal macrophages. All primer sequences can be found in Table S1. *IL-4Rα* mRNA in macrophages from MyIL4RαKO mice significantly decreased by 63% (*P*<0.0001) at baseline compared with FC mice (Figure 1A), and the decrease was confirmed at the protein level (Figure 1). When stimulated by IL-4, macrophages from MyIL4RαKO mice showed significantly diminished expression of AAM markers, including *Arg1* (6.2-fold decrease), *Ym1* (6.5-fold decrease) and *Relmα/Fizz1* (resistin-like molecule α; 7.7-fold decrease; Figure 1B). In addition to IL-4, we also used IL-10 and/or IL-13 to induce alternative macrophage activation to confirm that AAM polarization is blunted in IL4RαKO mice. When exposed to IL-13 or IL-13 plus IL-10, but not IL-10 alone, the expressions of *Arg1*, *Ym1*, and *Fizz1* mRNA were consistently suppressed by IL-4Rα deficiency (Figure S1). In contrast to the AAM markers, IL4RαKO macrophages showed 1.6-fold to 1.9-fold (*P*<0.001) significantly increased expression in CAM markers including *TNFα* (tumor necrosis factor α; 1.9-fold increase), *IL-1β* (1.75-fold increase), and *IL-6* (1.6-fold increase) when stimulated by LPS (Figure 1C). Taken together, these results suggest that myeloid IL-4Rα deficiency significantly inactivates IL-4Rα signaling in macrophages in vitro.

Alternative Macrophage Activation Is Attenuated in MyIL4RαKO Mice In Vivo

We next investigated the role of MyIL4Rα in AAM polarization in vivo. Specifically, we performed flow cytometric sorting to isolate macrophages from the heart of FC and MyIL4RαKO mice and then characterized macrophage polarization by quantitative reverse transcription–polymerase chain reaction. We found, as expected, that MyIL4RαKO mice exhibited an abrogated expression of *IL-4Rα* (Figure 2A). Consistent with in vitro data, macrophages from the hearts of AngII/salt-treated MyIL4RαKO mice also exhibited a significant 3-fold to 5-fold (*P*<0.001) decrease in the gene expression of AAM markers including *Arg1* (5.3 times decrease; *P*<0.0001), *Ym1* (3.1 times decrease; *P*<0.0001), and *Fizz1* (3.2 times decrease; *P*<0.001), compared with the corresponding macrophages from FC mice (Figure 2A). Moreover, the decrease of Arg1 and Ym1 was confirmed at the protein level by immunohistochemical staining. Arg1-positive areas, as well as Ym1-positive areas, in the heart sections of AngII/salt-treated MyIL4RαKO mice were ≈2-fold lower than those of the corresponding FC mice (Figure 2B and 2C).
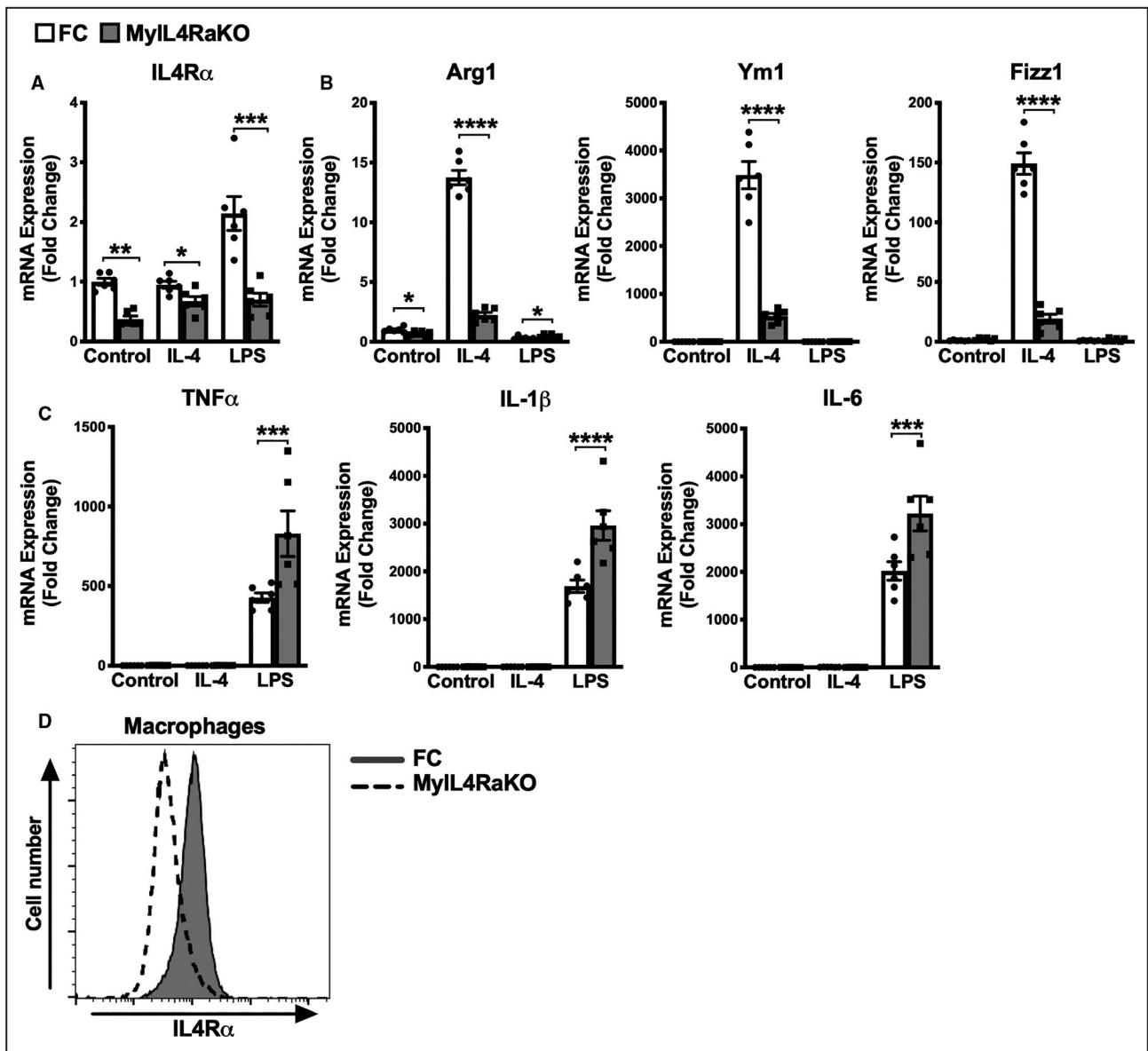
Figure 1. Myeloid-specific IL-4Rα knockout inactivates IL-4Rα signaling in peritoneal macrophages in vitro.
Peritoneal macrophages were isolated from control and MyIL4RaKO mice and then stimulated with IL-4 for 24 hours or LPS for 3 hours. mRNA levels of (**A**) *IL-4Rα*; (**B**) AAM markers *Arg1, Ym1,* and *Relmα/Fizz1*; and (**C**) CAM markers *TNFα, IL-1β,* and *IL-6* were measured by quantitative reverse transcription–polymerase chain reaction. Results are presented as mean±SEM. n=6 per group. *P<0.05, **P<0.01, ***P<0.001, ****P<0.0001. **D**, Expression of IL-4Rα in peritoneal macrophages of indicated mice were monitored by flow cytometry. Representative of at least 3 independent experiments. AAM indicates alternatively activated macrophage; *Arg1*, arginase 1; CAM, classically activated macrophage; FC, floxed control; IL, interleukin; IL-4Rα, interleukin-4 receptor α; LPS, lipopolysaccharide; MyIL4RaKO, myeloid-specific IL-4Rα knockout; *Relma/Fizz1*, resistin-like molecule α; *TNFα*, tumor necrosis factor α; and *Ym1*, chitinase 3-like 3.

We also measured the AAM-associated marker CD206 and CAM-associated marker TNFα in macrophages from both the heart and aorta by flow cytometry. The percentage of TNFα+CD206− and TNFα−CD206+ macrophage populations were comparable between FC and MyIL4RαKO mice, whether in the sham or AngII/salt group (Figure S2). Despite these comparable proportions, there were significant increases in the absolute numbers of TNFα+CD206− and TNFα−CD206+ macrophages in AngII/salt-treated hearts and aortas compared with those of sham mice (Figure S2C and S2F), which suggests the AngII/salt-induced infiltration of macrophages in the hearts and aortas. Among the multiple AAM markers that we tested, CD206 is the sole marker that is comparable between macrophages from FC and MyIL4RαKO
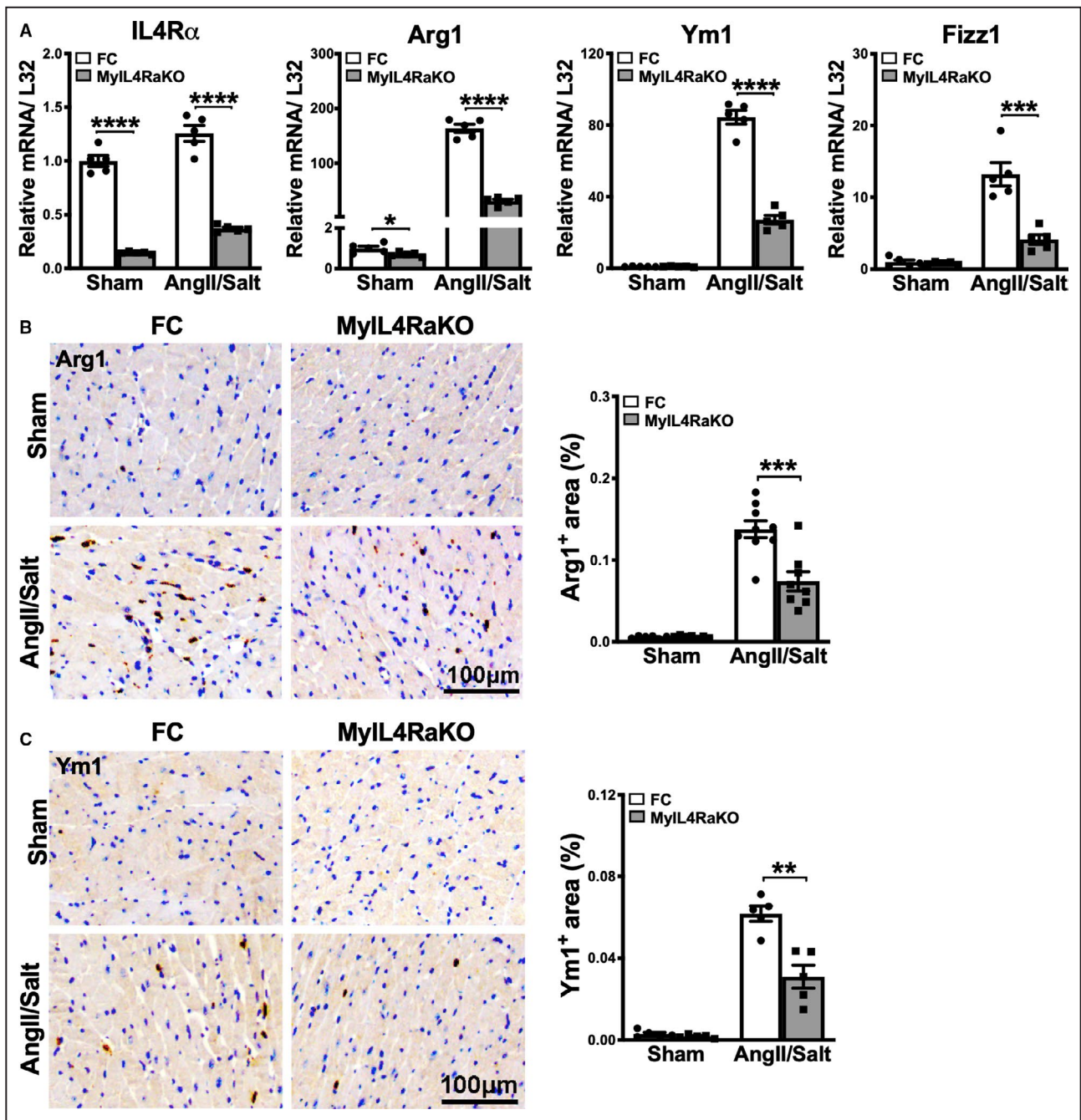
Figure 2.   Myeloid-specific IL-4Rα deficiency attenuates alternative macrophage activation in AngII/salt–induced cardiac remodeling in vivo.

A, Gene expression analysis of CD11b+F4/80+ macrophages sorted by flow cytometry from indicated hearts. mRNA levels of *IL-4Rα* and M2-like (alternatively activated) macrophage markers *Arg1, Ym1*, and *Relmα/Fizz1* were determined using quantitative reverse transcription–polymerase chain reaction. Pooled samples of 4 sham mice or 2 AngII/salt–treated mice are shown. Each dot represents 1 RNA sample from the pooled mice. n=5 per group. **B**, Representative pictures of Arg1-stained heart sections with or without exposure to AngII/salt (bar=100 μm). The percentage of Arg1-positive areas in indicated hearts was quantified and is shown on the right (n=6–9 per group). **C**, Representative images of Ym1-stained heart sections with or without AngII/salt treatment (bar=100 μm). Quantification of the percentage of Ym1-positive areas is shown on the right (n=5 per group). Results are presented as mean±SEM. *P<0.05; **P<0.01; ***P<0.001; ****P<0.0001. AngII/Salt indicates angiotensin II and high salt; Arg1, arginase 1; FC, floxed control; IL-4Rα, interleukin-4 receptor α; MyIL4RaKO, myeloid-specific IL-4Rα knockout; *Relmα/Fizz1*, resistin-like molecule α; and Ym1, chitinase 3-like 3.

mice. AAM markers Arg1 and Ym1 significantly decreased in macrophages from MyIL4RαKO mice in both mRNA and protein levels compared with FC mice (Figure 2). Overall, the weight of evidence indicates that IL-4Rα expression within myeloid cells controls AAM markers. These results also highlight the necessity of using a panel of markers to characterize alternative macrophage activation instead of 1 single marker such as CD206.

Overall, these results indicate that myeloid IL-4Rα deficiency significantly attenuates the alternative macrophage activation during AngII/salt-induced cardiovascular remodeling, although the expression of CD206 was not changed.

Myeloid IL-4Rα Deficiency Protects Against AngII/Salt-Induced Cardiovascular Dysfunction

To test whether myeloid IL-4Rα signaling would functionally affect the pathophysiology of cardiovascular remodeling during hypertension, we subjected MyIL4RαKO and FC mice to AngII/salt for 4 weeks.[22,23] AngII/salt significantly increased the arterial pressure and heart rate, but no differences were detected as a result of myeloid-specific IL-4Rα deficiency (Figure 3A and 3B). AngII/salt resulted in significantly reduced ejection fraction and fractional shortening in FC mice; however, these responses were substantially mitigated in MyIL4RαKO mice (Figure 3C). In MyIL4RαKO mice, ejection fraction and fractional shortening after AngII/salt exposure were even comparable with the sham group (Figure 3C). In addition, compared with FC, MyIL4RαKO mice showed significant decreases in systolic and diastolic LV areas, LV end systolic and diastolic diameters, LV end systolic and diastolic volumes, and systole and diastole LV posterior wall thicknesses, indicating a stronger potential for cardiac contraction (Figure 3). MyIL4RαKO mice also displayed improved aortic function as indicated by significantly increased aorta velocity peak gradient (Figure 3E), and this was associated with preservation of the ascending aorta diameter (Figure 3E). These data indicate that myeloid IL-4Rα signaling is importantly involved in cardiac functional change induced by AngII/salt, and myeloid IL-4Rα deficiency preserves cardiac function even after the pathophysiological changes caused by AngII/salt.

Myeloid IL-4Rα Deficiency Does Not Affect AngII/Salt-Induced Cardiovascular Hypertrophy

To identify the mechanism by which myeloid IL-4Rα deficiency protects against AngII/salt-induced

cardiac functional decline, we first assessed whether disruption of myeloid IL-4Rα signaling affected cardiovascular hypertrophy. Hence, we measured cardiac mass and cardiomyocyte size. Both cardiac mass and cardiomyocyte size were significantly increased in response to AngII/salt; however, no differences were detected between FC and MyIL4RαKO mice (Figure S3A and S3B). We then analyzed vascular hypertrophy by measuring the wall thickness and medial area of the aorta. Similarly, AngII/salt significantly increased aortic wall thickness and aortic medial area, but no differences were found between FC and MyIL4RαKO mice (Figure S3C). These results indicate that myeloid IL-4Rα signaling is not involved in cardiac or vascular hypertrophic remodeling caused by AngII/salt.

Myeloid IL-4Rα Deficiency Does Not Extensively Affect AngII/Salt-Induced Inflammatory Responses

To determine if myeloid IL-4Rα signaling regulates the inflammatory responses during AngII/salt-induced cardiovascular remodeling, we measured the expression of inflammatory genes in the heart and aorta of MyIL4RαKO and FC mice. In the heart, gene expressions of inflammatory cytokines including TNFα, IL-1β, and IL-6 were significantly upregulated by AngII/salt; however, there were no significant differences between AngII/salt-treated FC and MyIL4RαKO mice (Figure S4A). Notably, ablation of myeloid IL-4Rα enhanced basal inflammation in the heart with increased *TNFα* and *IL-6* mRNA expression in sham MyIL4RαKO mice compared with sham FC mice (Figure S4A).

In the aorta, *TNFα, IL-1β*, and *IL-6* mRNA levels were also increased after AngII/salt exposure (Figure S4C), but they were differently regulated by myeloid IL-4Rα signaling. Specifically, compared with AngII/salt-treated FC mice, aortic *TNFα* mRNA was increased and *IL-6* mRNA was decreased in MyIL4RαKO mice, whereas *IL-1β* mRNA were similar when compared with FC mice (Figure S4C), indicating a gene-dependent role of myeloid IL-4Rα in inflammatory responses in AngII/salt-treated aorta.

Hypertension induced by AngII/salt promote reactive oxygen species production.[24–26] We next investigated whether myeloid IL-4Rα signaling contributes to oxidative stress induced by AngII/salt by measuring the gene expression of reactive oxygen species–related genes, including *CYBA* (neutrophil cytochrome b light chain/p22phox), *NCF1* (neutrophil cytosolic factor 1/p47phox), and *Nox4* (nicotinamide adenine dinucleotide phosphate oxidase 4) in the heart and aorta. All 3 genes were significantly upregulated in response to AngII/salt except *Nox4*

in the aorta; however, no differences were detected between AngII/salt-treated MyIL4RαKO and FC mice (Figure S4). It should be noted that *p22phox* and *Nox4* mRNA levels were increased in the hearts of sham MyIL4RαKO mice compared with sham FC mice (Figure S4).

Figure 3.   Myeloid-specific IL-4Rα deficiency preserves cardiac function in AngII/salt–induced cardiovascular injury.
A, The systolic and diastolic BP and MAP of sham mice and mice subjected to AngII/salt (n=5–6 per group) were determined. Quantitative evaluations of cardiac function by echocardiography are shown and include (**B**) heart rate; (**C**) EF, FS, and systolic and diastolic LV areas; (**D**) LVESD, LVEDD, LVESV, and LVEDV; and (**E**) LVPWTs, LVPWTd, aorta velocity peak gradient, and ascending aorta diameter (n=7 to 11 per group). Results are shown as mean±SEM. *P<0.05; **P<0.01; ***P<0.001; ****P<0.0001. **F**, Representative echocardiographic images in sham or AngII/salt–treated FC and MyIL4RaKO mice. AngII/Salt indicates angiotensin II and high salt; BP, blood pressure; EF, ejection fraction; FC, floxed control; FS, fractional shortening; IL-4Rα, interleukin-4 receptor α; LV, left ventricle; LVEDD, LV end diastolic diameter; LVESD, LV end systolic diameter; LVEDV, LV end diastolic volume; LVESV, LV end systolic volume; LVPWTd, diastole LV posterior wall thickness; LVPWTs, systole LV posterior wall thickness; MAP, mean arterial pressure; and MyIL4RaKO, myeloid-specific IL-4Rα knockout.

We next examined whether myeloid IL-4Rα signaling regulates immune cell infiltration into the heart and aorta in response to AngII/salt by assessing macrophage numbers by flow cytometry. As expected, macrophages were significantly increased in response to AngII/salt in both the heart and aorta; however, there was no difference between FC and MyIL4RαKO mice (Figure S5), which suggests that myeloid IL-4Rα signaling does not substantially contribute to macrophage infiltration in these tissues during hypertension. As IL-4Rα was also abolished in monocytes (Figure S6A and S6B), and infiltrating macrophages can be derived from monocytes, we also examined the role of IL-4Rα signaling in AngII/salt-induced monocyte recruitment by measuring monocytes in the blood and spleen with flow cytometry. In monocytes, we also analyzed Ly6C^{low} and Ly6C^{high} subpopulations separately. Myeloid IL-4Rα deficiency did not change the distribution of Ly6C^{low} or Ly6C^{high} monocytes in total monocytes, but it did cause a slight ≈30% increase in the number of total circulating monocytes after AngII/salt treatment (Figure S6C and S6D). In the spleen, myeloid IL-4Rα deficiency neither changed the distribution of Ly6C^{low} or Ly6C^{high} monocytes in the total monocyte pool nor the total number of monocytes (Figure S6E and S6F).

As MyIL4RαKO mice exhibited a 72% reduction of IL-4Rα on circulating neutrophils (Figure S7A and S7B), we measured AngII/salt-induced neutrophil infiltration in the heart and aorta and circulating neutrophils by flow cytometry. There was no difference in AngII/salt-induced neutrophil infiltration between FC and MyIL4RαKO mice (Figure S7C through S7F). Similarly, circulating neutrophils were also comparable between AngII/salt-exposed FC and MyIL4RαKO mice; however, both the percentage of neutrophils and neutrophil numbers in blood were increased 1.5-fold in sham MyIL4RαKO mice compared with sham FC mice (Figure S7G and S7H). Finally, T cells contribute to AngII-induced hypertension,[27,28] so we measured T cells in the heart, aorta, and blood. There was no difference in either the percentage or the number of T cells between FC and MyIL4RαKO mice (Figure S7), so it is clear that myeloid IL-4Rα signaling is not involved in T cell regulation.

Myeloid IL-4Rα Signaling Plays an Important Role in Fibrotic Remodeling

As IL-4 signaling promotes cardiac fibrosis,[9,10] we next tested whether myeloid-specific IL-4Rα deficiency impacts cardiac fibrosis induced by AngII/salt treatment. We found that both interstitial (1.9-fold decrease) and perivascular fibrosis (1.4-fold decrease) were significantly decreased in AngII/salt-exposed MyIL4RαKO mice (P<0.01) compared with FC mice (Figure 4A and 4B). Aortic fibrosis was also significantly diminished in MyIL4RαKO mice compared with FC mice (Figure 4C). These results indicate that myeloid IL-4Rα signaling contributes to AngII/salt-induced fibrosis in the heart and aorta.

Prolonged hypertension also causes end-organ kidney damage[29–33] attributed to fibrosis. We next examined if myeloid-specific IL-4Rα deficiency impacts kidney fibrosis during AngII/salt treatment. We found a significant reduction in renal fibrosis in MyIL4RαKO mice compared with FC mice (P<0.01; Figure S8). This result suggests that myeloid IL-4Rα signaling promotes kidney fibrosis in addition to fibrosis in the myocardium and aorta during AngII/salt treatment.

IL-4Rα-Deficient Macrophages Contribute to the Decreased Fibrosis in MyIL4RαKO Mice

We measured the expression of fibrosis-related genes including *TGFβ1* (transforming growth factor β1), *PDGFα* (platelet-derived growth factor α), *BMP9* (bone morphogenetic protein 9), and *TIMP1* and *MMPs* in fluorescence-activated cell sorting macrophages by quantitative reverse transcription–polymerase chain reaction. Compared with macrophages from FC mice, *TGFβ1* was significantly downregulated (≈1.7-fold) in macrophages from MyIL4RαKO mice before and after AngII/salt treatment (Figure 5A). In addition, the expression of the profibrotic genes *PDGFα* and *TIMP1* were ≈2-fold decreased in macrophages from AngII/salt-treated MyIL4RαKO mice compared with control macrophages (Figure 5A). In contrast, antifibrotic genes were significantly upregulated in
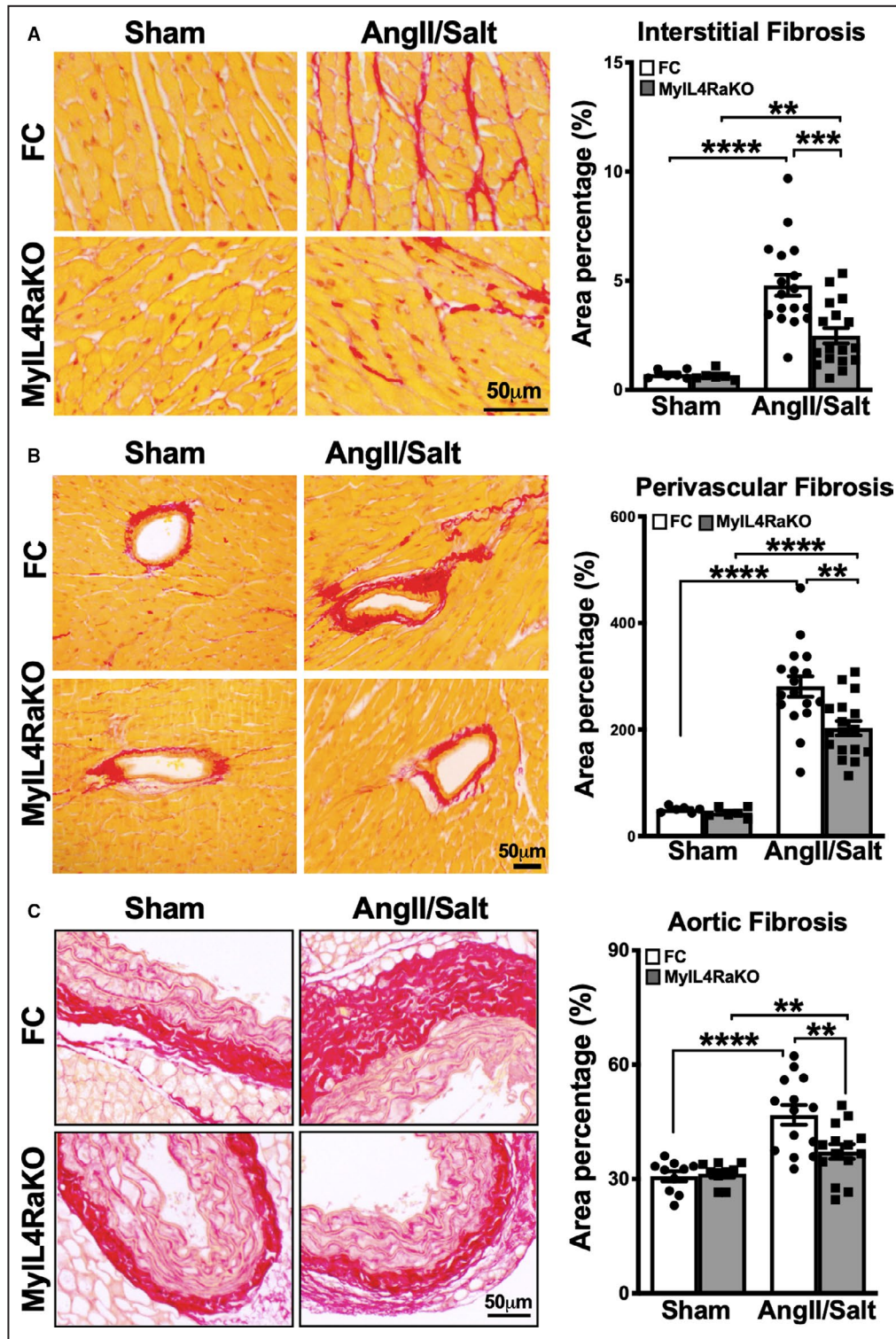
Figure 4.   IL-4Rα deficiency in myeloid cells suppresses fibrosis.
A, Representative images of picrosirius red-stained cardiac interstitial fibrosis (red) induced by AngII/salt and quantification of cardiac interstitial fibrosis: sham mice, n=6 per group; AngII/salt-treated mice, n=17 per group. **B**, Representative images of picrosirius red-stained perivascular fibrosis (red) induced by AngII/salt and quantification of perivascular fibrosis in the heart: sham mice, n=6 per group; AngII/salt-treated mice, n=17 per group. **C**, Representative images of picrosirius red-stained aorta sections and quantification of fibrotic area percentage in sham and AngII/salt-treated mice (n=9–14 per group). Results are shown as mean±SEM (bar=50 μm). **P<0.01; ***P<0.001; ****P<0.0001. AngII/Salt indicates angiotensin II and high salt; FC, floxed control; IL-4Rα, interleukin-4 receptor α; and MyIL4RaKO, myeloid-specific IL-4Rα knockout.
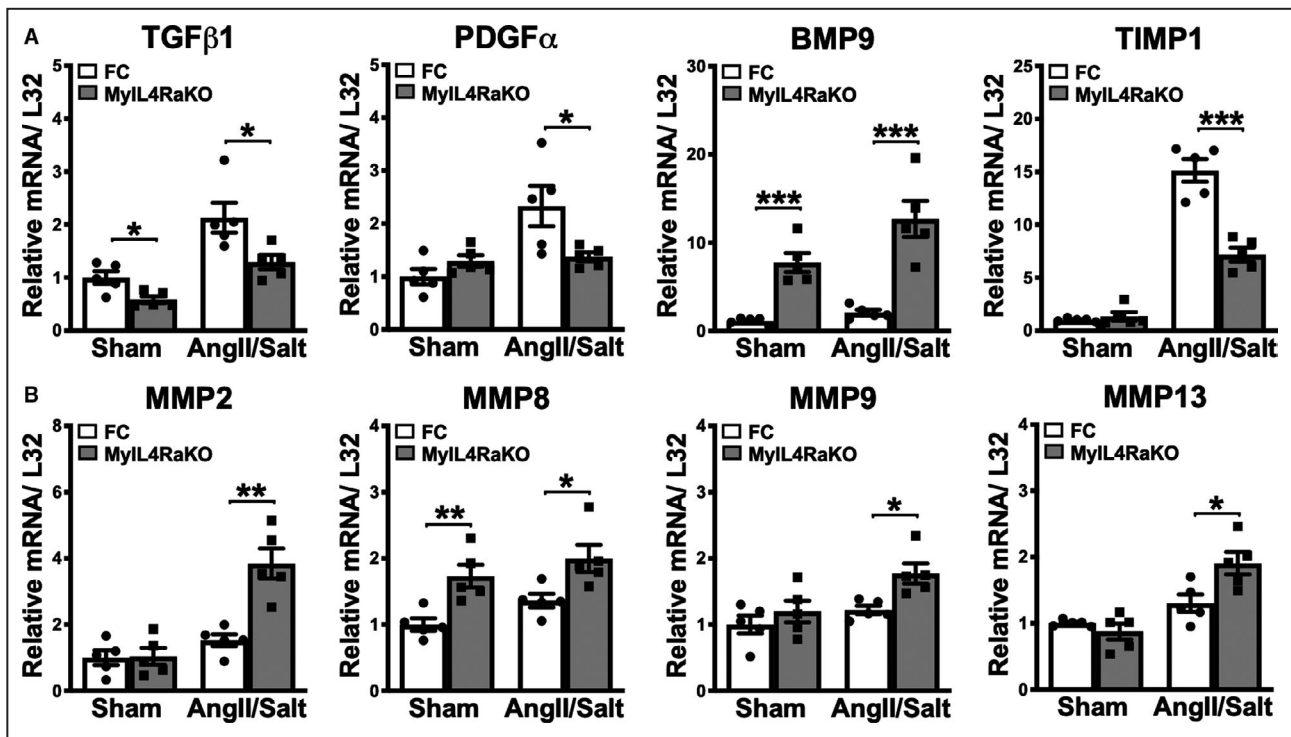
Figure 5. Myeloid-specific IL-4Rα deficiency downregulates profibrotic but upregulates antifibrotic gene expression in macrophages from AngII/salt-treated mice.

Gene expression analysis of CD11b⁺F4/80⁺ macrophages sorted by flow cytometry from the hearts of sham or AngII/salt-treated FC and MyIL4RaKO mice. mRNA levels of the (**A**) fibrosis-related genes *TGFβ1*, *PDGFα*, and *BMP9* and the MMP inhibitor *TIMP1* and (**B**) *MMP2*, *MMP8*, *MMP9*, and *MMP13*. Macrophages were pooled from 4 sham mice or 2 AngII/salt-treated mice. Each dot represents 1 RNA sample from the pooled macrophages (n=5 per group). Results are presented as mean±SEM. *$P<0.05$; **$P<0.01$; ***$P<0.001$. AngII/Salt indicates angiotensin II and high salt; *BMP9*, bone morphogenetic protein 9; FC, floxed control; IL-4Rα, interleukin-4 receptor α; MMP, matrix metalloproteinase; MyIL4RaKO, myeloid-specific IL-4Rα knockout; *PDGFα*, platelet-derived growth factor α; *TGFβ1*, transforming growth factor β1; and *TIMP1*, tissue inhibitor of metalloproteinase 1.

macrophages from AngII/salt-treated MyIL4RαKO mice, including *BMP9* (6.1 times increase, also in sham-treated mice), *MMP2* (2.5 times increase), *MMP8* (1.5 times increase, also in sham-treated mice), *MMP9* (1.45 times increase), and *MMP13* (1.46 times increase) compared with control macrophages (Figure 5A and 5B). In sum, these results suggest that myeloid IL-4Rα signaling regulates AngII/salt-induced fibrosis by controlling gene expression in macrophages.

We also measured fibrosis-related genes and proteins from hearts and aortas. In the heart, we found that profibrotic genes including *Col3A1* (collagen type III α 1 chain), *Gal3* (galectin-3), and *TIMP1* exhibited a 1.7 to 2.5 times decrease in MyIL4RαKO mice compared with FC mice (Figure 6A and 6B) in response to AngII/salt treatment. The antifibrotic genes *BMP9* and *MMP10* were significantly increased in the hearts of MyIL4RαKO mice compared with FC hearts (Figure 6A and 6B). Although no difference was shown in *MMP2* mRNA between AngII/salt-treated FC and MyIL4RαKO mice, *MMP2* mRNA was significantly higher in sham

MyIL4RαKO mice than sham FC mice (Figure 6B). We further complemented our gene expressions results by Western blot analysis, which demonstrated that the MMP10 protein was significantly increased in the hearts of MyIL4RαKO compared with FC mice with or without AngII/salt treatment (Figure 6C). Moreover, the TIMP1 protein was significantly decreased in MyIL4RαKO compared with FC mice with or without AngII/salt treatment (Figure 6C).

In the aorta, both *TGFβ1* and *TIMP1* mRNA were significantly downregulated in AngII/salt-treated MyIL4RαKO mice compared with corresponding FC aortas (Figure 7A). Antifibrotic genes, including *BMP9*, *MMP2*, *MMP3*, and *MMP10* exhibited a 1.6-fold to 2-fold increase in the aortas of AngII/salt-treated MyIL4RαKO mice compared with similarly treated FC mice (Figure 7A and 7B). *BMP9* and *MMP10* mRNA levels were also increased 2-fold to 4-fold in the aortas of sham MyIL4RαKO mice compared with sham FC mice (Figure 7A and 7B). Furthermore, we found increased MMP3 and MMP10 proteins in the lysates of aortas from MyIL4RαKO mice compared with FC mice (Figure 7C).
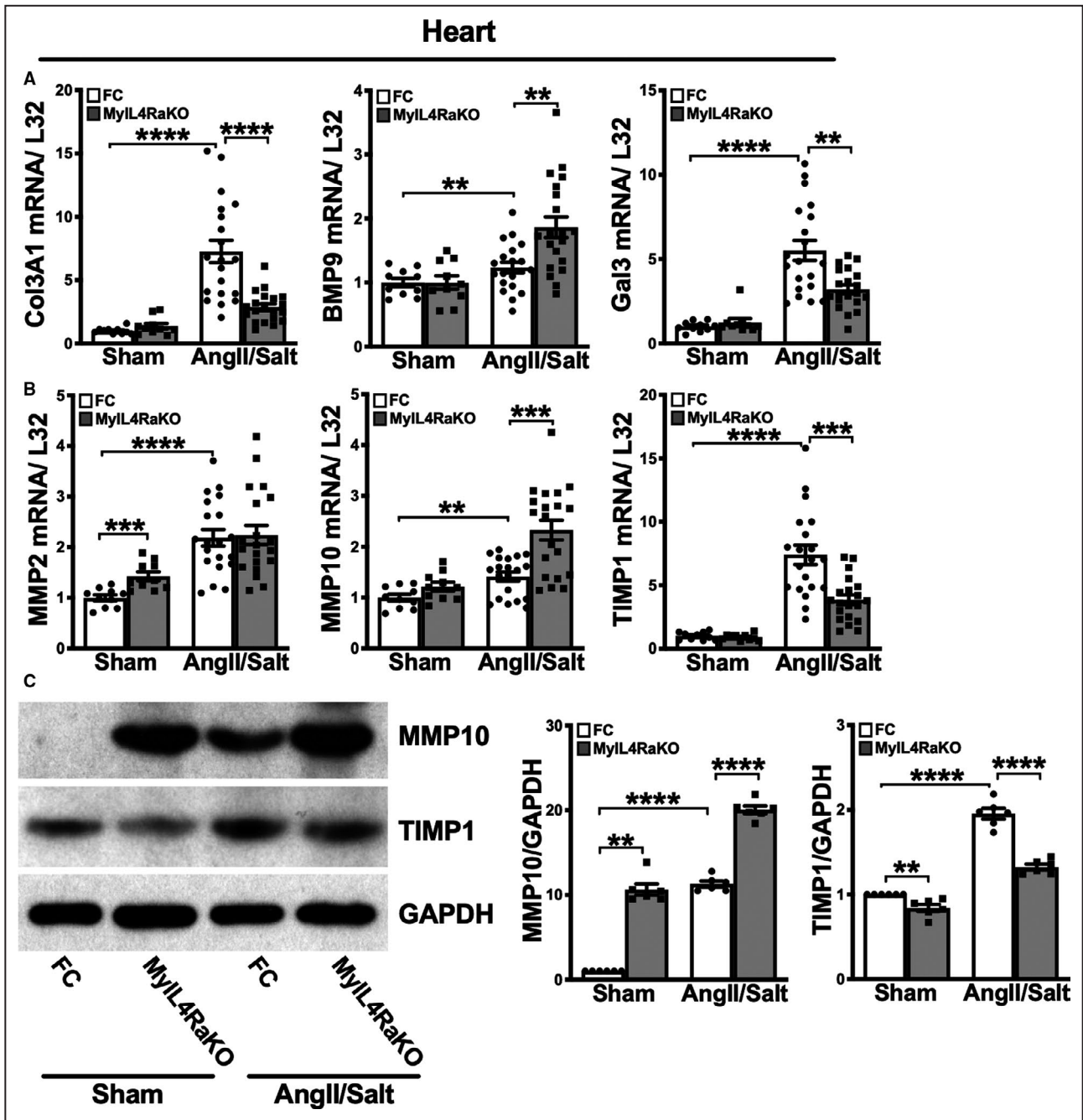
Figure 6. **Myeloid-specific IL-4Rα deficiency diminishes profibrotic but enhances antifibrotic signaling in hearts.**
A, mRNA levels of the fibrosis-related genes *Col3A1*, *BMP9*, and *Gal3* were determined in the heart tissues of sham and AngII/salt-treated mice. **B**, Gene expressions of *MMP2* and *MMP10* and the MMP inhibitor *TIMP1* in heart tissues were measured by quantitative reverse transcription–polymerase chain reaction: sham, n=10 per group; AngII/salt, n=20 per group. **C**, Protein levels of MMP10 and TIMP1 in the tissue lysates of hearts from sham or AngII/salt-treated mice were determined by Western blot. GAPDH was used as an internal control. Quantification of MMP10 and TIMP1 protein levels are shown on the right (n=6 per group). Results are shown as mean±SEM. **$P<0.01$; ***$P<0.001$; ****$P<0.0001$. AngII/Salt indicates angiotensin II and high salt; *BMP9*, bone morphogenetic protein 9; *Col3A1*, collagen type III alpha 1 chain; FC, floxed control; *Gal3*, galectin-3; IL-4Rα, interleukin-4 receptor α; MMP, matrix metalloproteinase; MyIL4RaKO, myeloid-specific IL-4Rα knockout; and *TIMP1*, tissue inhibitor of metalloproteinase 1.

Taken together, these results suggest that macrophage IL-4Rα contributes to AngII/salt-induced fibrosis by upregulating profibrotic genes and downregulating antifibrotic genes.

DISCUSSION

Hypertension causes adverse cardiovascular remodeling, including fibrosis, long-lasting chronic inflammation, and
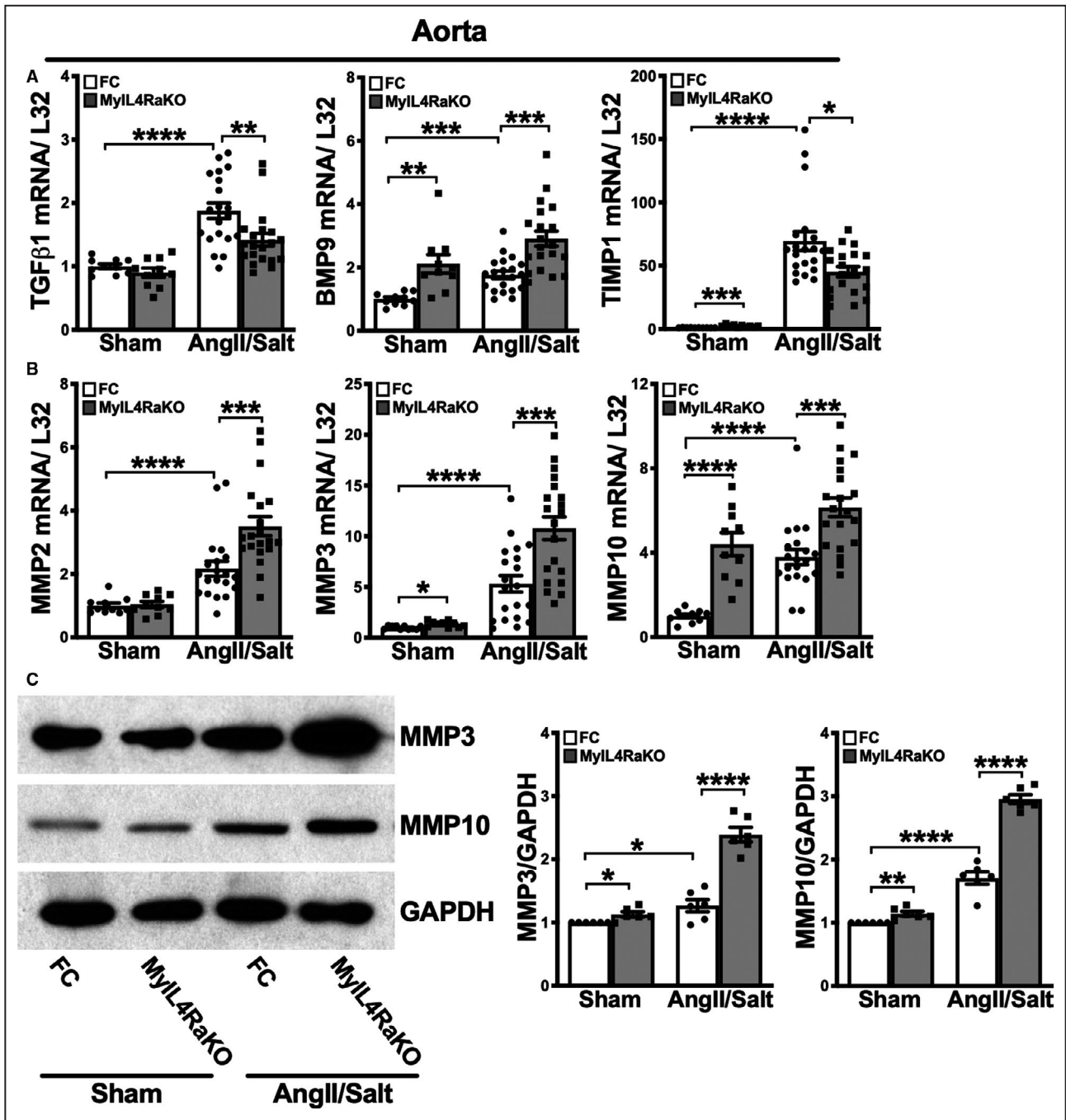
Figure 7. **Myeloid-specific IL-4Rα deficiency downregulates profibrotic but upregulates antifibrotic signaling in aorta.**
A, mRNA levels of the fibrosis-related genes *TGFβ1*, *BMP9*, and *TIMP1* were determined in the aortas of sham and AngII/salt-treated mice. **B**, Gene expressions of *MMP2*, *MMP3*, and *MMP10* in the aorta were measured by quantitative reverse transcription–polymerase chain reaction (sham, n=10 per group; AngII/salt, n=20 per group). **C**, Protein levels of MMP3 and MMP10 in the tissue lysates of aortas from sham or AngII/salt-treated mice were determined by Western blot. GAPDH was used as the loading control. Quantification of the MMP3 and MMP10 protein levels are shown on the right (n=6 per group). Results are shown as mean±SEM. *$P<0.05$; **$P<0.01$; ***$P<0.001$; ****$P<0.0001$. AngII/Salt indicates angiotensin II and high salt; *BMP9*, bone morphogenetic protein 9; FC, floxed control; IL-4Rα, interleukin-4 receptor α; MMP, matrix metalloproteinase; MyIL4RaKO, myeloid-specific IL-4Rα knockout; *TGFβ1*, transforming growth factor β1; and *TIMP1*, tissue inhibitor of metalloproteinase 1.

hypertrophic structural changes in the LV.[34] Modifying the adverse remodeling is a potential strategy to prevent cardiovascular diseases. In this study, we show that

blocking myeloid-specific IL-4Rα signaling inhibits AngII/salt-induced profibrotic remodeling and preserves cardiac function by suppressing alternative macrophage activation.

Macrophage polarization plays a critical role in cardiovascular remodeling.[4] There is a wide spectrum of macrophage polarization with 2 extreme phenotypes: CAM and AAM. Generally, CAMs are proinflammatory, and AAMs are profibrotic.[35,36] In our study, we found myeloid-specific IL-4Rα deficiency suppressed AAMs both in vitro and in vivo (Figures 1 and 2). As macrophage heterogeneity and plasticity have been recognized in recent years,[37] 1 single CAM or AAM marker is often not enough to define macrophage phenotype. For example, in our study, we used Arg1, Ym1, and Fizz1 to determine the attenuated alternative macrophage activation in MyIL4RαKO mice. Given the complexity of macrophage polarization, it is important to describe macrophage phenotypes with multiple markers. Importantly, the present M1/M2 paradigm is limited as this paradigm is based on the controlled conditions of in vitro culture, which does not reflect the complexity of in vivo conditions.[38] Possibly in vivo, M1 and M2 status of macrophages may exist in a continuum.[39] It will be interesting in the future to develop markers that characterize the intermediates which lie between M1 and M2 status. In addition, there could be a dynamic change in the macrophage polarization on a stimulus such as AngII/salt, so it is worth pursuing early and late macrophage phenotypic responses to follow the temporal macrophage polarization switch. In our study, we used 4 weeks as the experimental end point because 4 weeks and 8 weeks are commonly used as end points of an AngII-induced hypertension model,[9,23,28] and there is no significant phenotypic difference between 4-week and 8-week timepoints in C57BL/6 male mice exposed to AngII and a high-salt diet.[40] In the future, including both early and late time points to investigate the involvement of macrophage polarization in cardiovascular remodeling could reveal a dynamic picture of macrophage phenotypes.

The impact of AAM suppression in AngII/salt-induced cardiovascular remodeling was investigated in our study. Mice that were subjected to AngII/salt displayed increased heart weight, enlarged cardiomyocytes, and expanded vascular walls, which is consistent with previous reports that AngII/salt induces hypertrophy.[41,42] However, no hypertrophic difference was shown between FC and MyIL4Rα mice, which is also consistent with the report that global IL-4 deficiency does not affect hypertrophy.[9] These results together suggest that myeloid IL-4Rα signaling and AAM activation are not involved in cardiovascular hypertrophic remodeling. In contrast, myeloid IL-4Rα deficiency-induced AAM suppression resulted in fibrosis decrease.

Fibrosis plays a critical role in cardiovascular remodeling. It can be reparative or detrimental depending on the specific disease model.[43] Appropriate and proper fibrosis is beneficial during wound healing and tissue repair[44–46]; however, unnecessary fibrosis leads to deleterious functional disorders.[47–49] In our study, myeloid IL-4Rα deficiency diminishes harmful fibrosis and protects against cardiac dysfunction induced by AngII/salt (Figure 3). We also found fibrosis in MyIL4Rα mice is decreased through an imbalance of profibrotic and antifibrotic signaling pathways (Figures 5 through 7), where fibroblasts could be potentially involved. Fibroblasts are a central effector cell type in fibrosis. During cardiovascular remodeling, macrophages activate mesenchymal cells including fibroblasts.[50] Persistent activation by profibrotic signalings, such as TGFβ (transforming growth factor β) released by macrophages, drives quiescent fibroblasts to proliferate and transdifferentiate.[51] Communication between macrophages and fibroblasts, together with T helper 2 responses, sustain profibrotic remodeling. We found that myeloid IL-4Rα deficiency blunts TGFβ signaling, shown by decreased *TGFβ1* and *PDGFα* expression in IL-4Rα-deficient macrophages. These results suggests that myeloid IL-4Rα signaling regulates fibrosis partially by controlling fibroblasts proliferation and transdifferentiation, which should be examined in the future.

In conclusion, our study has revealed that myeloid IL-4Rα signaling contributes to cardiovascular profibrotic remodeling induced by AngII/salt, and myeloid cells are important cellular targets of endogenous IL-4Rα signaling. Our results suggest that targeting myeloid IL-4Rα signaling could suppress excessive profibrotic remodeling and protect cardiovascular function during hypertension.

Supplementary Material

Table S1
Figures S1–S8

REFERENCES

1. Harvey A, Montezano AC, Lopes RA, Rios F, Touyz RM. Vascular fibrosis in aging and hypertension: molecular mechanisms and clinical implications. *Can J Cardiol*. 2016;32:659–668. DOI: 10.1016/j.cjca.2016.02.070.

2. Frangogiannis NG. The immune system and the remodeling infarcted heart: cell biological insights and therapeutic opportunities. *J Cardiovasc Pharmacol*. 2014;63:185–195. DOI: 10.1097/FJC.0000000000000003.

3. Shinagawa H, Frantz S. Cellular immunity and cardiac remodeling after myocardial infarction: role of neutrophils, monocytes, and macrophages. *Curr Heart Fail Rep*. 2015;12:247–254. DOI: 10.1007/s11897-015-0255-7.

4. Frieler RA, Mortensen RM. Immune cell and other noncardiomyocyte regulation of cardiac hypertrophy and remodeling. *Circulation*. 2015;131:1019–1030. DOI: 10.1161/CIRCULATIONAHA.114.008788.

5. Troidl C, Möllmann H, Nef H, Masseli F, Voss S, Szardien S, Willmer M, Rolf A, Rixe J, Troidl K, et al. Classically and alternatively activated macrophages contribute to tissue remodelling after myocardial infarction. *J Cell Mol Med*. 2009;13:3485–3496. DOI: 10.1111/j.1582-4934.2009.00707.x.

6. Vergadi E, Chang MS, Lee C, Liang OD, Liu X, Fernandez-Gonzalez A, Mitsialis SA, Kourembanas S. Early macrophage recruitment and alternative activation are critical for the later development of hypoxia-induced pulmonary hypertension. *Circulation*. 2011;123:1986–1995. DOI: 10.1161/CIRCULATIONAHA.110.978627.

7. Xue J, Sharma V, Hsieh MH, Chawla A, Murali R, Pandol SJ, Habtezion A. Alternatively activated macrophages promote pancreatic fibrosis in chronic pancreatitis. *Nat Commun*. 2015;6:7158. DOI: 10.1038/ncomms8158.

8. Diny NL, Baldeviano GC, Talor MV, Barin JG, Ong S, Bedja D, Hays AG, Gilotra NA, Coppens I, Rose NR, et al. Eosinophil-derived IL-4 drives progression of myocarditis to inflammatory dilated cardiomyopathy. *J Exp Med*. 2017;214:943–957. DOI: 10.1084/jem.20161702.

9. Peng H, Sarwar Z, Yang XP, Peterson EL, Xu J, Janic B, Rhaleb N, Carretero OA, Rhaleb NE. Profibrotic role for interleukin-4 in cardiac remodeling and dysfunction. *Hypertension*. 2015;66:582–589. DOI: 10.1161/HYPERTENSIONAHA.115.05627.

10. Kanellakis P, Ditiatkovski M, Kostolias G, Bobik A. A pro-fibrotic role for interleukin-4 in cardiac pressure overload. *Cardiovasc Res*. 2012;95:77–85. DOI: 10.1093/cvr/cvs142.

11. Kirstein F, Nieuwenhuizen NE, Jayakumar J, Horsnell WG, Brombacher F. Role of IL-4 receptor alpha-positive CD4(+) T cells in chronic airway hyperresponsiveness. *J Allergy Clin Immunol*. 2016;137:1852–1862.e1859. DOI: 10.1016/j.jaci.2015.10.036.

12. Ratthe C, Pelletier M, Chiasson S, Girard D. Molecular mechanisms involved in interleukin-4-induced human neutrophils: expression and regulation of suppressor of cytokine signaling. *J Leukoc Biol*. 2007;81:1287–1296. DOI: 10.1189/jlb.0306209.

13. Girard D. Phenotypic and functional change of neutrophils activated by cytokines utilizing the common cytokine receptor gamma chain. *Chem Immunol Allergy*. 2003;83:64–80. DOI: 10.1159/000071565.

14. Girard D, Paquin R, Beaulieu AD. Responsiveness of human neutrophils to interleukin-4: induction of cytoskeletal rearrangements, de novo protein synthesis and delay of apoptosis. *Biochem J*. 1997;325:147–153. DOI: 10.1042/bj3250147.

15. Doucet C, Brouty-Boye D, Pottin-Clemenceau C, Jasmin C, Canonica GW, Azzarone B. IL-4 and IL-13 specifically increase adhesion molecule and inflammatory cytokine expression in human lung fibroblasts. *Int Immunol*. 1998;10:1421–1433. DOI: 10.1093/intimm/10.10.1421.

16. Horsnell WG, Vira A, Kirstein F, Mearns H, Hoving JC, Cutler AJ, Dewals B, Myburgh E, Kimberg M, Arendse B, et al. IL-4ralpha-responsive smooth muscle cells contribute to initiation of TH2 immunity and pulmonary pathology in *Nippostrongylus brasiliensis* infections. *Mucosal Immunol*. 2011;4:83–92.

17. O'Meara CC, Wamstad JA, Gladstone RA, Fomovsky GM, Butty VL, Shrikumar A, Gannon JB, Boyer LA, Lee RT. Transcriptional reversion of cardiac myocyte fate during mammalian cardiac regeneration. *Circ Res*. 2015;116:804–815. DOI: 10.1161/CIRCRESAHA.116.304269.

18. Herbert DR, Hölscher C, Mohrs M, Arendse B, Schwegmann A, Radwanska M, Leeto M, Kirsch R, Hall P, Mossmann H, et al. Alternative macrophage activation is essential for survival during schistosomiasis and downmodulates T helper 1 responses and immunopathology. *Immunity*. 2004;20:623–635. DOI: 10.1016/S1074-7613(04)00107-4.

19. Weber DS, Rocic P, Mellis AM, Laude K, Lyle AN, Harrison DG, Griendling KK. Angiotensin II-induced hypertrophy is potentiated in mice overexpressing p22phox in vascular smooth muscle. *Am J Physiol Heart Circ Physiol*. 2005;288:H37–H42. DOI: 10.1152/ajpheart.00638.2004.

20. Castoldi G, Di Gioia C, Bombardi C, Perego C, Perego L, Mancini M, Leopizzi M, Corradi B, Perlini S, Zerbini G, et al. Prevention of myocardial fibrosis by N-acetyl-seryl-aspartyl-lysyl-proline in diabetic rats. *Clin Sci*. 2009;118:211–220. DOI: 10.1042/CS20090234.

21. Hu D, Yin C, Mohanta SK, Weber C, Habenicht AJ. Preparation of single cell suspensions from mouse aorta. *Bio Protoc*. 2016;6:e1832. DOI: 10.21769/BioProtoc.1832.

22. Lerman LO, Chade AR, Sica V, Napoli C. Animal models of hypertension: an overview. *J Lab Clin Med*. 2005;146:160–173. DOI: 10.1016/j.lab.2005.05.005.

23. Zhao X, Pollock DM, Zeldin DC, Imig JD. Salt-sensitive hypertension after exposure to angiotensin is associated with inability to upregulate renal epoxygenases. *Hypertension*. 2003;42:775–780. DOI: 10.1161/01.HYP.0000085649.28268.DF.

24. Harrison DG, Gongora MC. Oxidative stress and hypertension. *Med Clin North Am*. 2009;93:621–635. DOI: 10.1016/j.mcna.2009.02.015.

25. Baradaran A, Nasri H, Rafieian-Kopaei M. Oxidative stress and hypertension: possibility of hypertension therapy with antioxidants. *J Res Med Sci*. 2014;19:358–367.

26. Guzik TJ, Touyz RM. Oxidative stress, inflammation, and vascular aging in hypertension. *Hypertension*. 2017;70:660–667. DOI: 10.1161/HYPERTENSIONAHA.117.07802.

27. Guzik TJ, Hoch NE, Brown KA, McCann LA, Rahman A, Dikalov S, Goronzy J, Weyand C, Harrison DG. Role of the T cell in the genesis of angiotensin II induced hypertension and vascular dysfunction. *J Exp Med*. 2007;204:2449–2460. DOI: 10.1084/jem.20070657.

28. Crowley SD, Song YS, Lin EE, Griffiths R, Kim HS, Ruiz P. Lymphocyte responses exacerbate angiotensin II-dependent hypertension. *Am J Physiol Regul Integr Comp Physiol*. 2010;298:R1089–R1097. DOI: 10.1152/ajpregu.00373.2009.

29. Kirchhoff F, Krebs C, Abdulhag UN, Meyer-Schwesinger C, Maas R, Helmchen U, Hilgers KF, Wolf G, Stahl RA, Wenzel U. Rapid development of severe end-organ damage in C57BL/6 mice by combining DOCA salt and angiotensin II. *Kidney Int*. 2008;73:643–650. DOI: 10.1038/sj.ki.5002689.

30. Kumar V, Wollner C, Kurth T, Bukowy JD, Cowley AW Jr. Inhibition of mammalian target of rapamycin complex 1 attenuates salt-induced hypertension and kidney injury in Dahl salt-sensitive rats. *Hypertension*. 2017;70:813–821. DOI: 10.1161/HYPERTENSIONAHA.117.09456.

31. Mehrotra P, Patel JB, Ivancic CM, Collett JA, Basile DP. Th-17 cell activation in response to high salt following acute kidney injury is associated with progressive fibrosis and attenuated by AT-1R antagonism. *Kidney Int*. 2015;88:776–784. DOI: 10.1038/ki.2015.200.

32. Fiebeler A, Nussberger J, Shagdarsuren E, Rong S, Hilfenhaus G, Al-Saadi N, Dechend R, Wellner M, Meiners S, Maser-Gluth C, et al. Aldosterone synthase inhibitor ameliorates angiotensin II-induced organ damage. *Circulation*. 2005;111:3087–3094. DOI: 10.1161/CIRCULATIONAHA.104.521625.

33. Lea WB, Kwak ES, Luther JM, Fowler SM, Wang Z, Ma J, Fogo AB, Brown NJ. Aldosterone antagonism or synthase inhibition reduces end-organ damage induced by treatment with angiotensin and high salt. *Kidney Int*. 2009;75:936–944. DOI: 10.1038/ki.2009.9.

34. Messerli FH, Rimoldi SF, Bangalore S. The transition from hypertension to heart failure: contemporary update. *JACC Heart Fail* 2017;5:543–551.

35. Wynn TA, Ramalingam TR. Mechanisms of fibrosis: therapeutic translation for fibrotic disease. *Nat Med*. 2012;18:1028–1040. DOI: 10.1038/nm.2807.

36. Moore JP, Vinh A, Tuck KL, Sakkal S, Krishnan SM, Chan CT, Lieu M, Samuel CS, Diep H, Kemp-Harper BK, et al. M2 macrophage accumulation in the aortic wall during angiotensin II infusion in mice is associated with fibrosis, elastin loss, and elevated blood pressure. *Am J Physiol Heart Circ Physiol*. 2015;309:H906–H917. DOI: 10.1152/ajpheart.00821.2014.

37. Morganti JM, Riparip LK, Rosi S. Call off the Dog(ma): M1/M2 polarization is concurrent following traumatic brain injury. *PLoS One*. 2016;11:e0148001. DOI: 10.1371/journal.pone.0148001.

38. Nahrendorf M, Swirski FK. Abandoning M1/M2 for a network model of macrophage function. *Circ Res*. 2016;119:414–417. DOI: 10.1161/CIRCR ESAHA.116.309194.

39. Martinez FO, Gordon S. The M1 and M2 paradigm of macrophage activation: time for reassessment. *F1000Prime Rep*. 2014;6:13.

40. Gonzalez GE, Rhaleb NE, D'Ambrosio MA, Nakagawa P, Liu Y, Leung P, Dai X, Yang XP, Peterson EL, Carretero OA. Deletion of interleukin-6 prevents cardiac inflammation, fibrosis and dysfunction without affecting blood pressure in angiotensin II-high salt-induced hypertension. *J Hypertens*. 2015;33:144–152. DOI: 10.1097/HJH.0000000000000358.

41. Takayanagi T, Forrester SJ, Kawai T, Obama T, Tsuji T, Elliott KJ, Nuti E, Rossello A, Kwok HF, Scalia R, et al. Vascular ADAM17 as a novel therapeutic target in mediating cardiovascular hypertrophy and perivascular fibrosis induced by angiotensin II. *Hypertension*. 2016;68:949–955. DOI: 10.1161/HYPERTENSIONAHA.116.07620.

42. Nakamura T, Kataoka K, Fukuda M, Nako H, Tokutomi Y, Dong YF, Ichijo H, Ogawa H, Kim-Mitsuyama S. Critical role of apoptosis signal-regulating kinase 1 in aldosterone/salt-induced cardiac inflammation and fibrosis. *Hypertension*. 2009;54:544–551. DOI: 10.1161/HYPER TENSIONAHA.109.135392.

43. Talman V, Ruskoaho H. Cardiac fibrosis in myocardial infarction-from repair and remodeling to regeneration. *Cell Tissue Res*. 2016;365:563–581. DOI: 10.1007/s00441-016-2431-9.

44. Shiraishi M, Shintani Y, Shintani Y, Ishida H, Saba R, Yamaguchi A, Adachi H, Yashiro K, Suzuki K. Alternatively activated macrophages determine repair of the infarcted adult murine heart. *J Clin Invest*. 2016;126:2151–2166. DOI: 10.1172/JCI85782.

45. Knipper JA, Willenborg S, Brinckmann J, Bloch W, Maass T, Wagener R, Krieg T, Sutherland T, Munitz A, Rothenberg ME, et al. Interleukin-4 receptor alpha signaling in myeloid cells controls collagen fibril assembly in skin repair. *Immunity*. 2015;43:803–816. DOI: 10.1016/j.immuni.2015.09.005.

46. Song J, Frieler RA, Whitesall SE, Chung Y, Vigil T, Muir LA, Ma J, Brombacher F, Goonewardena SN, Lumeng CN, et al. Myeloid interleukin-4 receptor alpha (IL4ralpha) is essential in post-myocardial infarction healing by regulating inflammation and fibrotic remodeling. *Am J Physiol Heart Circ Physiol*. 2021;320:H323–H337. DOI: 10.1152/ajphe art.00251.2020.

47. Matsubara LS, Matsubara BB, Okoshi MP, Cicogna AC, Janicki JS. Alterations in myocardial collagen content affect rat papillary muscle function. *Am J Physiol Heart Circ Physiol*. 2000;279:H1534–H1539. DOI: 10.1152/ajpheart.2000.279.4.H1534.

48. Narayan S, Janicki JS, Shroff SG, Pick R, Weber KT. Myocardial collagen and mechanics after preventing hypertrophy in hypertensive rats. *Am J Hypertens*. 1989;2:675–682. DOI: 10.1093/ajh/2.9.675.

49. Yamamoto K, Masuyama T, Sakata Y, Nishikawa N, Mano T, Yoshida J, Miwa T, Sugawara M, Yamaguchi Y, Ookawara T, et al. Myocardial stiffness is determined by ventricular fibrosis, but not by compensatory or excessive hypertrophy in hypertensive heart. *Cardiovasc Res*. 2002;55:76–82. DOI: 10.1016/S0008-6363(02) 00341-3.

50. Frangogiannis NG. The inflammatory response in myocardial injury, repair, and remodelling. *Nat Rev Cardiol*. 2014;11:255–265. DOI: 10.1038/nrcardio.2014.28.

51. Gong D, Shi W, Yi SJ, Chen H, Groffen J, Heisterkamp N. TGFβ signaling plays a critical role in promoting alternative macrophage activation. *BMC Immunol*. 2012;13:31.

SUPPLEMENTAL MATERIAL

Table S1. Sequences of primers used in this study.

| Gene	Forward	Reverse
Arg1	ACCTGGCCTTTGTTGATGTCCCTA	AGAGATGCTTCCAACTGCCAGACT
BMP9	CAGAACTGGGAACAAGCATCC	GCCGCTGAGGTTTAGGCTG
Col3A1	CCTGGCTCAAATGGCTCAC	CAGGACTGCCGTTATTCCCG
Fizz1	ACTGCCTGTGCTTACTCGTTGACT	AAAGCTGGGTTCTCCACCTCTTCA
Gal3	GGAGAGGGAATGATGTTGCCT	TCCTGCTTCGTGTTACACACA
IL-6	GAGGATACCACTCCCAACAGACC	AAGTGCATCATCGTTGTTCATACA
IL-1β	AAGAGCTTCAGGCAGGCAGTATCA	TGCAGCTGTCTAATGGGAACGTCA
IL4Rα	TCTGCATCCCGTTGTTTTGC	GCACCTGTGCATCCTGAATG
L32	TTAAGCGAAACTGGCGGAAAC	TTGTTGCTCCCATAACCGATG
MMP2	CAAGTTCCCCGGCGATGTC	TTCTGGTCAAGGTCACCTGTC
MMP3	ACATGGAGACTTTGTCCCTTTTG	TTGGCTGAGTGGTAGAGTCCC
MMP8	TCTTCCTCCACACACAGCTTG	CTGCAACCATCGTGGCATTC
MMP9	GGACCCGAAGCGGACATTG	CGTCGTCGAAATGGGCATCT
MMP10	GAGCCACTAGCCATCCTGG	CTGAGCAAGATCCATGCTTGG
MMP13	CTTCTTCTTGTTGAGCTGGACTC	CTGTGGAGGTCACTGTAGACT
Nox4	ACTTTTCATTGGGCGTCCTC	AGAACTGGGTCCACAGCAGA
p22phox	TGCCAGTGTGATCTATCTGCT	TCGGCTTCTTTCGGACCTCT
p47phox	ACACCTTCATTCGCCATATTGC	TCGGTGAATTTTCTGTAGACCAC
PDGFα	GAGGAAGCCGAGATACCCC	TGCTGTGGATCTGACTTCGAG
TGFβ1	CTCCCGTGGCTTCTAGTGC	GCCTTAGTTTGGACAGGATCTG
TIMP1	CCTAGAGACACACCAGAGCA	TACCGGATATCTGCGGCATT
TNFα	CCCTCACACTCAGATCATCTTCT	GCTACGACGTGGGCTACAG
Ym1	CACCATGGCCAAGCTCATTCTTGT	TATTGGCCTGTCCTTAGCCCAACT

The primers were synthesized by Integrated DNA Technologies. L32, 60S ribosomal protein L32, was used as internal control.

**Figure S1. Myeloid IL4Rα knockout blunts IL-13- but not IL-10 induced alternative activation of macrophages.**
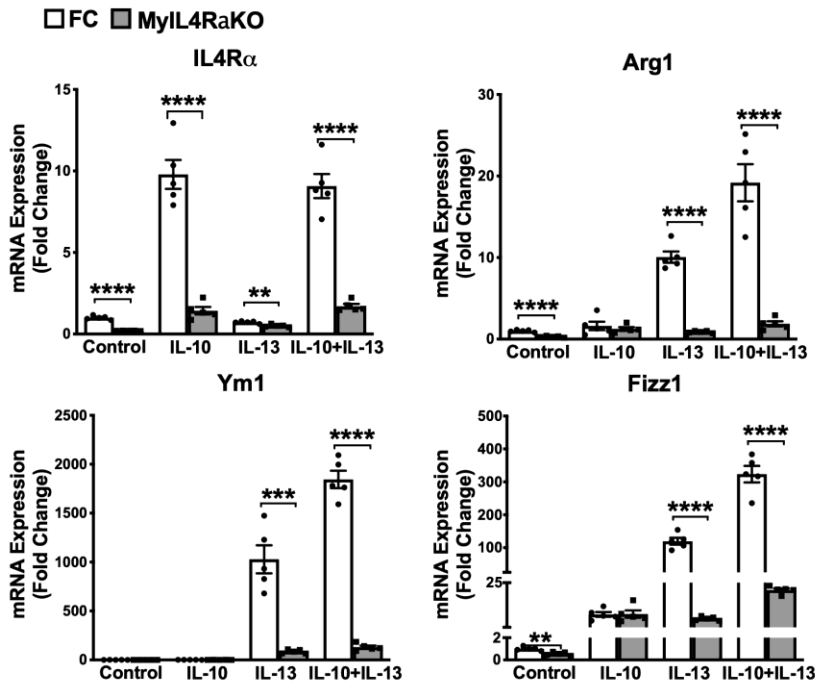
Peritoneal macrophages were isolated from FC and MyIL4RαKO mice and then alternatively stimulated with IL-10 (50ng/ml) or IL-13 (50ng/ml) or IL-10 and IL-13 for 24 hours. mRNA levels of IL4Rα and AAM markers including Arg1, Ym1 and Fizz1 were measured by qRT-PCR. Results are presented as means ± SEM. n=5 per group. **P <0.01; ***P <0.001, ****P < 0.0001.

**Figure S2. Myeloid-specific IL4Rα knockout does not change CD206⁺TNFα⁻ macrophage population *in vivo*.**
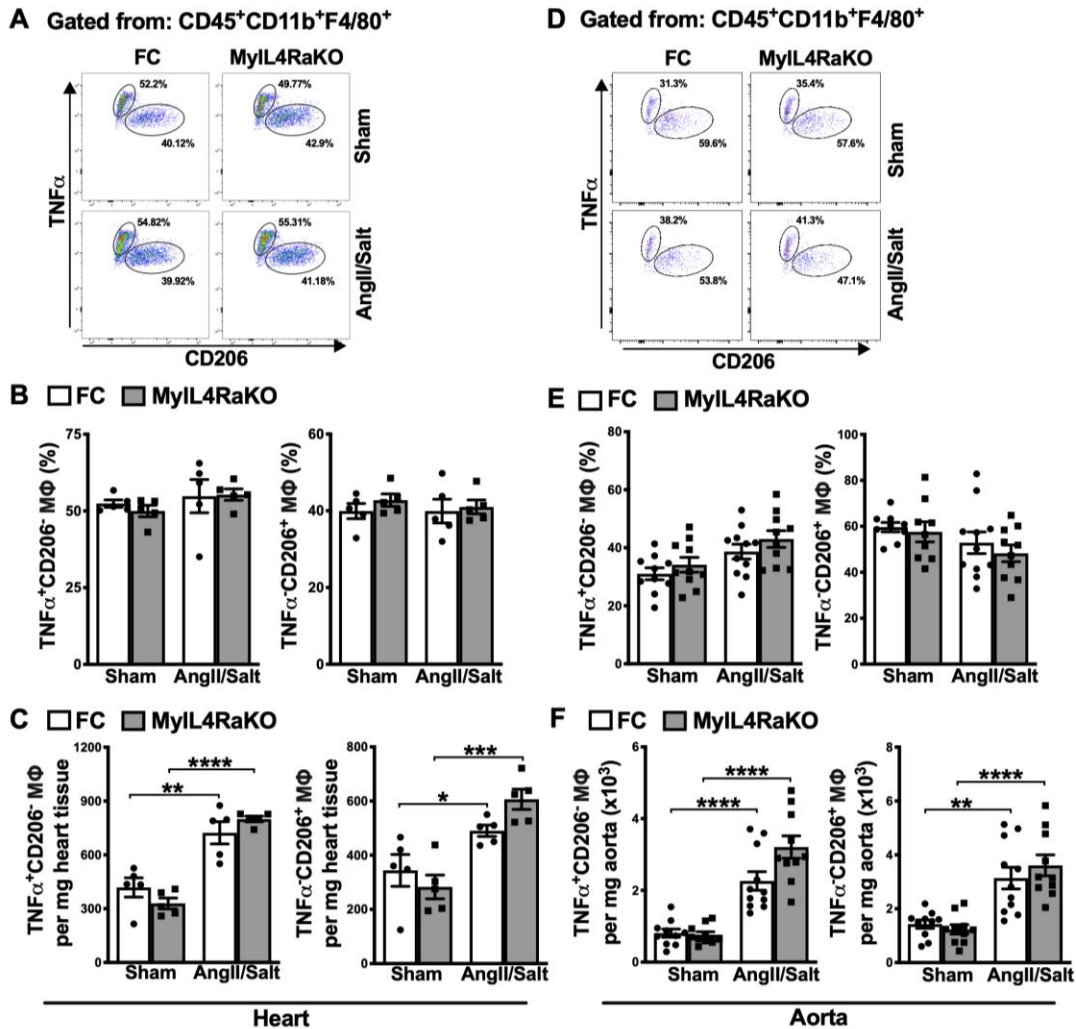
(A) Representative flow cytometry dot plots of CD206⁻TNFα⁺ and CD206⁺TNFα⁻ macrophages gated from macrophages in hearts. **(B)** Quantification of the percentage of CD206⁻TNFα⁺ and CD206⁺TNFα⁻ macrophages in total macrophages shown in (**A**). n=5 per group. **(C)** Quantification of CD206⁻TNFα⁺ and CD206⁺TNFα⁻ macrophage numbers from heart tissues. All cell numbers are expressed per milligram tissue. n=5 per group. **(D)** Representative flow cytometry dot plots of CD206⁻TNFα⁺ and CD206⁺TNFα⁻ macrophages gated from macrophages in aortas. **(E)** Quantification of the percentage of CD206⁻TNFα⁺ and CD206⁺TNFα⁻ macrophages in total macrophages shown in (**D**). n=10-11 per group. **(F)** Quantification of CD206⁻TNFα⁺ and CD206⁺TNFα⁻ macrophage numbers from aortas. All cell numbers are expressed per milligram tissue. n=10-11 per group. Results are shown as means ± SEM. *P <0.05; **P <0.01; ***P <0.001; ****P < 0.0001.

**Figure S3. Myeloid-specific IL4Rα knockout has no effect on cardiovascular hypertrophy.**
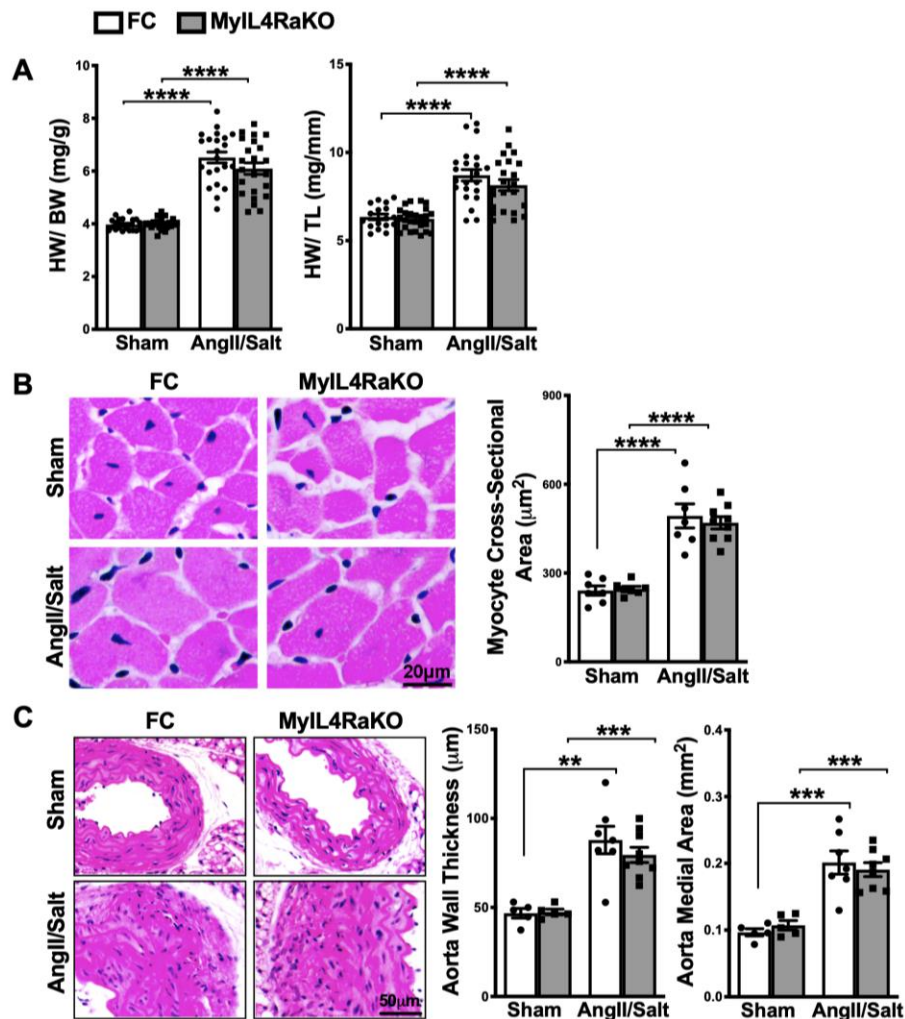
(A) Heart weight to body weight ratio (HW/BW, n=20-24 per group) and heart weight to tibia length ratio (HW/TL, n=17-25 per group) were measured to determine the cardiac hypertrophy during AngII/salt treatment. (B) Representative images of H&E stained heart sections and quantification of cardiomyocyte CSA (n=7-9 per group). (C) Representative photomicrograph of H&E stained aorta sections, and wall thickness and medial area of aorta (n=5-9 per group). Results are shown as means ± SEM. **P <0.01; ***P <0.001; ****P < 0.0001.

Figure S4. Inflammatory genes and ROS generation-related genes are mostly not affected by myeloid IL4Rα knockout.
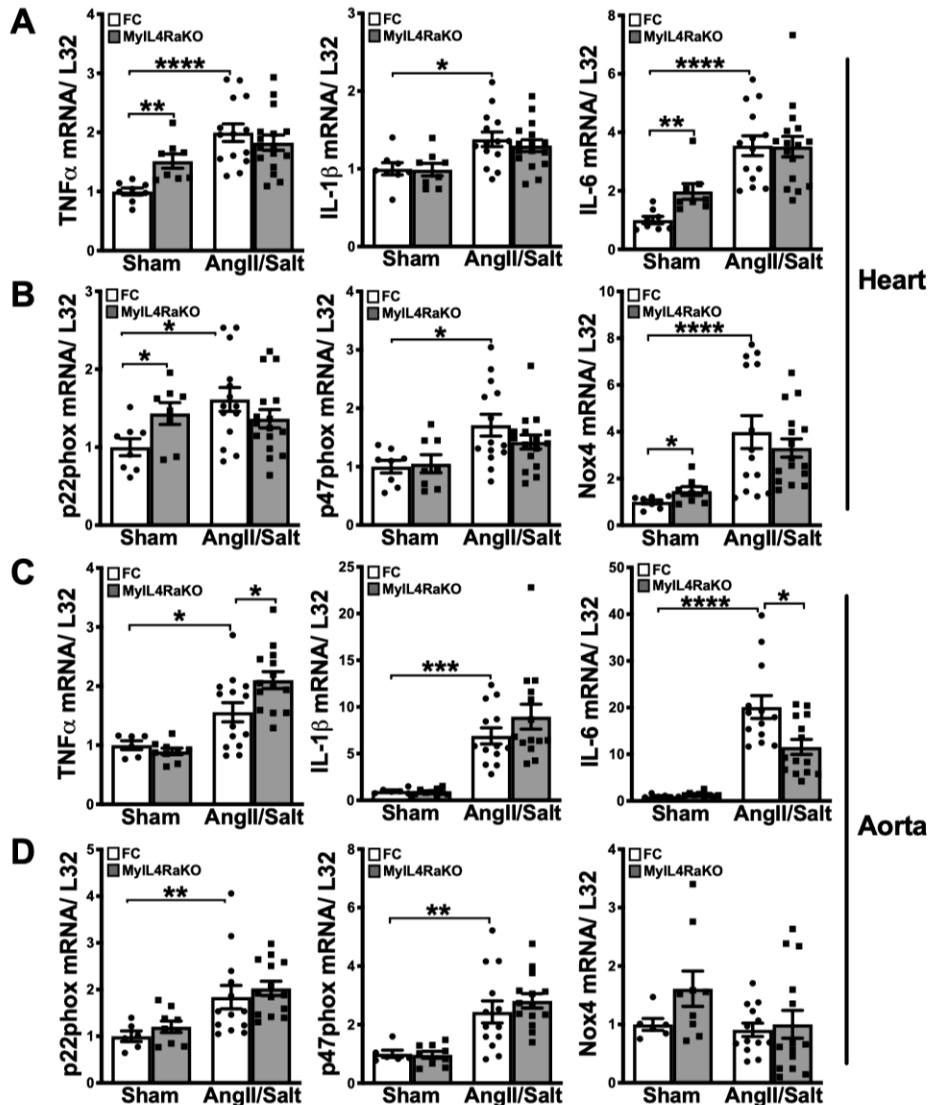

(A and C) The expression of inflammatory cytokines including TNFα, IL-1β and IL-6 at mRNA level was determined in **(A)** hearts and **(C)** aortas of sham and AngII/salt treated mice. **(B and D)** The expression of ROS generation related genes including p22phox, p47phox and Nox4 at mRNA level was determined in **(B)** hearts and **(D)** aortas of sham and AngII/salt treated mice. Results are shown as means ± SEM. Sham, n=6-9 per group; AngII/Salt, n=13-16 per group. *P <0.05; **P <0.01; ***P <0.001; ****P <0.0001.

Figure S5. Myeloid IL4Rα deficiency does not change macrophage recruitment induced by AngII and high salt.
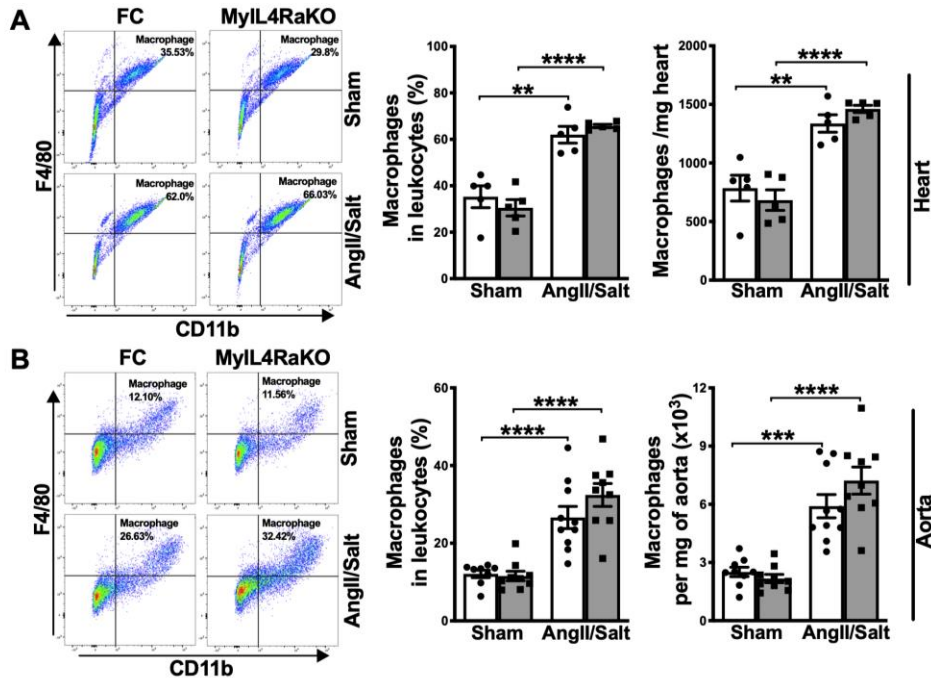
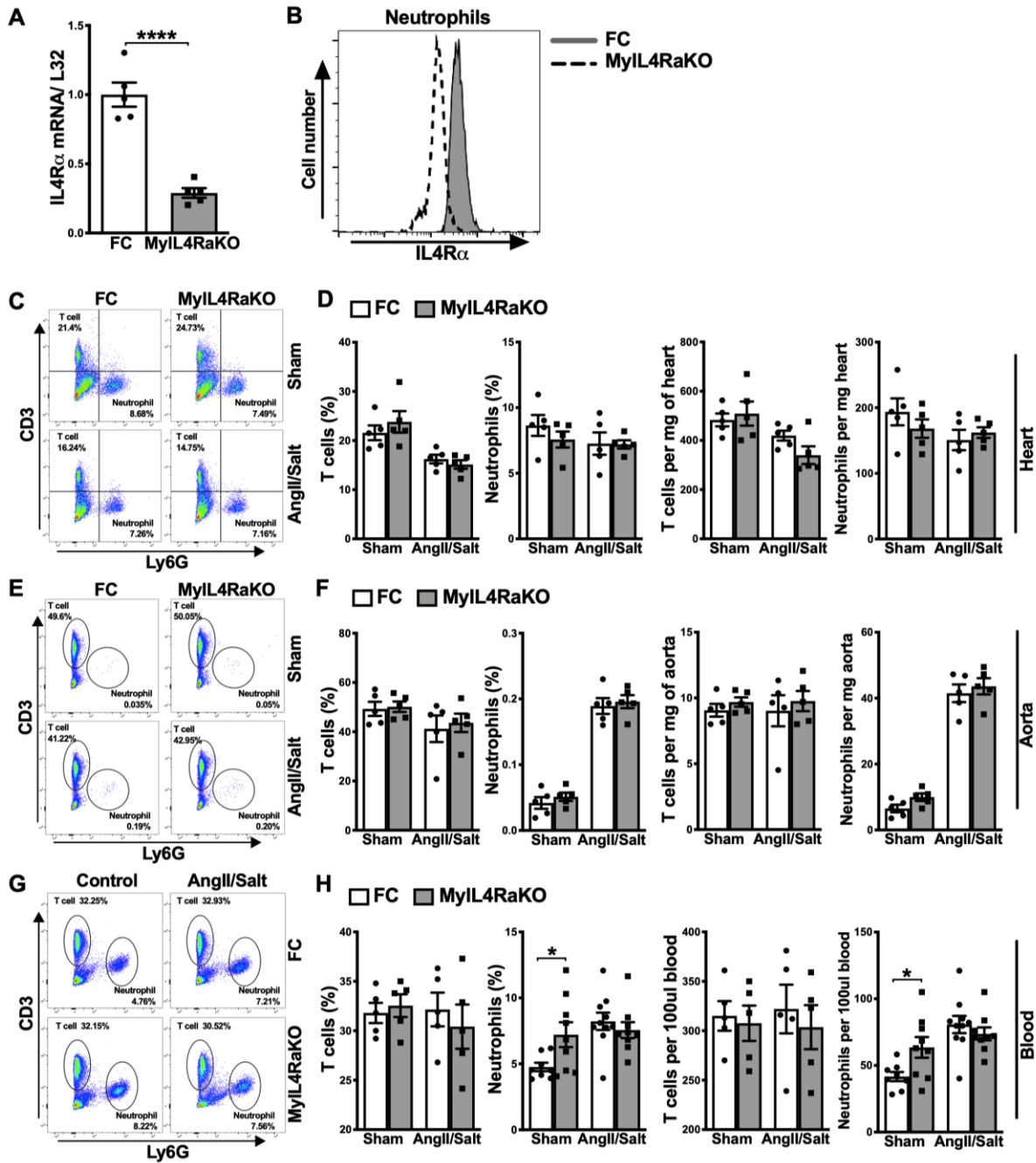

(A) Representative FACS dot plots of macrophages (CD11b$^+$F4/80$^+$) gated from leukocytes from heart tissues of sham and AngII and high salt-treated mice. The quantification of the percentage of macrophages in total leukocytes and macrophage numbers are shown on the right. n=5 per group. **(B)** Representative FACS dot plots of macrophages (CD11b$^+$F4/80$^+$) gated from leukocytes in aorta tissues of sham and AngII and high salt-treated mice. The quantification of the percentage of macrophages in leukocytes and macrophage numbers are shown on the right. n=9-10 per group. All cell numbers are expressed per milligram tissue. Results are shown as means ± SEM. **P <0.01; ***P <0.001; ****P < 0.0001.

Figure S6. Monocytes in blood and spleen in FC and MyIL4RαKO mice exposed to AngII/salt.
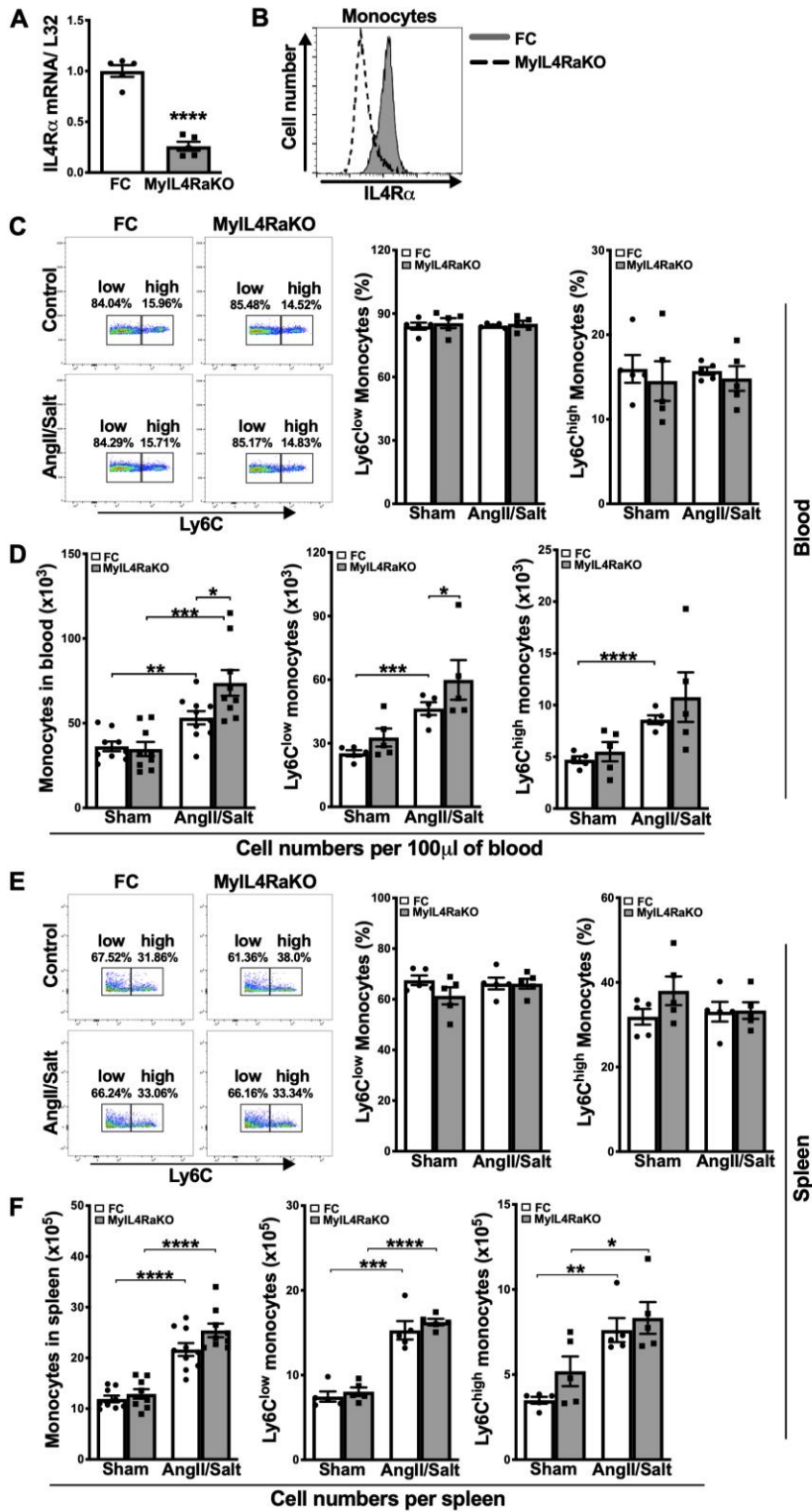
(A) mRNA levels of IL4Rα in monocytes sorted by flow cytometry from blood of FC and MyIL4RαKO mice. n=5 per group. **(B)** Expression of IL4Rα in circulating monocytes were monitored by flow cytometry. Representative of at least three independent experiments. **(C)** Representative FACS dot plots of Ly6C^{low} and Ly6C^{high} monocytes gated from total monocytes in blood. The percentage of Ly6C^{low} and Ly6C^{high} monocytes in total circulating monocytes is shown on the right. n=5 per group. **(D)** Total monocyte numbers (n=9-10 per group) and Ly6C^{low} and Ly6C^{high} monocyte numbers (n=5 per group) in 100μl blood. **(E)** Representative FACS dot plots of Ly6C^{low} and Ly6C^{high} monocytes gated from total monocytes in spleen. The percentage of Ly6C^{low} and Ly6C^{high} monocytes in total splenic monocytes is shown on the right. n=5 per group. **(F)** Total monocyte numbers (n=9-10 per group) and Ly6C^{low} and Ly6C^{high} monocyte numbers (n=5 per group) in the spleen. Results are shown as means ± SEM. *P <0.05; **P <0.01; ***P <0.001; ****P < 0.0001.

Figure S7. Myeloid IL4Rα deficiency does not change neutrophil and T cell recruitment induced by AngII and high salt.

(A) mRNA levels of IL4Rα in neutrophils sorted by flow cytometry from blood of FC and MyIL4RαKO mice. n=5. **(B)** Expression of IL4Rα in circulating neutrophils were monitored by flow cytometry. Representative of at least three independent experiments.

(C) Representative FACS dot plots of neutrophils (CD45$^+$CD11b$^+$Ly6G$^+$) and T cells (CD45$^+$CD3$^+$) from heart tissues of sham and AngII/salt-treated mice. **(D)** The quantification of the percentage of neutrophils and T cells in total leukocytes from hearts and neutrophil and T cell numbers. n=5. **(E)** Representative FACS dot plots of neutrophils (CD45$^+$CD11b$^+$Ly6G$^+$) and T cells (CD45$^+$CD3$^+$) from aorta tissues of sham and AngII/salt-treated mice. **(F)** The quantification of the percentage of neutrophils and T cells in total leukocytes from aortas and neutrophil and T cell numbers. n=5 per group. **(G)** Representative FACS dot plots of circulating neutrophils (CD45$^+$CD11b$^+$Ly6G$^+$) and T cells (CD45$^+$CD3$^+$) in sham and AngII/salt-treated mice. **(H)** The quantification of the percentage of neutrophils and T cells in total circulating leukocytes and circulating neutrophil and T cell numbers. n=5-10 per group. Results are shown as means ± SEM. *P <0.05; ****P < 0.0001.

Figure S8. Myeloid-specific IL4Rα deficiency reduces fibrosis in kidney.
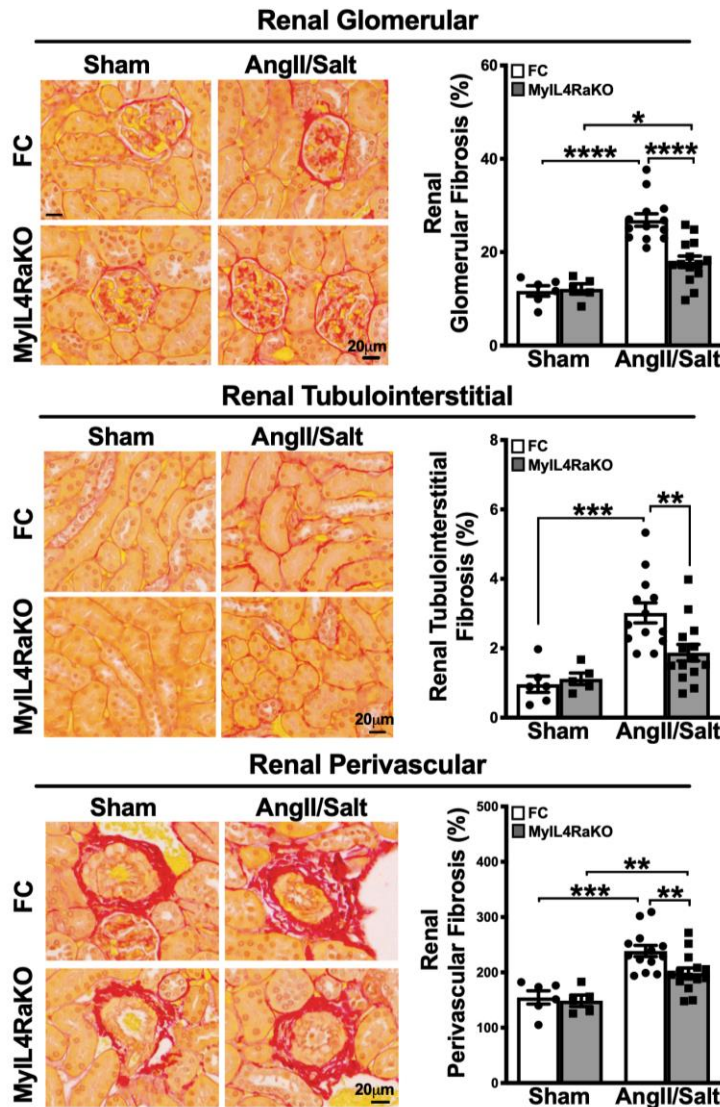
Representative images of glomerular, tubulointerstitial and perivascular region of picrosirius red stained kidney after exposure to AngII and high salt and the quantification of glomerular, tubulointerstitial and perivascular fibrosis. Sham mice: n=5-6 per group; AngII and high salt-treated mice: n=13-14 per group. Results are shown as means ± SEM. *P <0.05; **P <0.01; ***P <0.001; ****P < 0.0001.